Spring 1-1-2015

Laboratory Evaluation of Low-Temperature Thermally Enhanced Soil Vapor Extraction

Lauren Jane Reising
University of Colorado at Boulder, lauren.reising@colorado.edu

Laboratory Evaluation of Low-Temperature Thermally Enhanced Soil Vapor Extraction

by

Lauren Jane Reising

B.A., University of California, Berkeley

A thesis submitted to the

Faculty of the Graduate School of the

University of Colorado in partial fulfillment

of the requirements for the degree of

Masters of Science

Department of Civil, Environmental, and Architectural Engineering

2015

This thesis entitled:
Laboratory Evaluation of Low-Temperature Thermally Enhanced Soil Vapor Extraction
written by Lauren Jane Reising
has been approved for the Department of Civil, Environmental, and Architectural Engineering

Prof. John McCartney

Prof. Angela Bielefeldt

Prof. Dobroslav Znidarčić

Date

The final copy of this thesis has been examined by the signatories, and we find that both the content and the form meet acceptable presentation standards of scholarly work in the above mentioned discipline.

Reising, Lauren Jane (M.S. Civil Engineering)

Laboratory Evaluation of Low-Temperature Thermally Enhanced Soil Vapor Extraction

Thesis directed by Prof. John McCartney

The goal of this study is to understand the conditions in which heat collected from soil-borehole thermal energy storage (SBTES) systems can be used for thermally enhanced vapor extraction. SBTES systems consist of an array of closely-spaced vertical geothermal boreholes, and are used for storing heat collected from solar thermal panels. The temperature of the soil in these systems is expected to reach values ranging from 40 to 60 °C. Although thermal enhancement of soil-vapor extraction (SVE) has been investigated in several studies, they typically involved temperatures in the range of 100-300 °C and the role of relatively low temperatures such as those in SBTES systems has not been thoroughly evaluated. Although the temperature is not significant, the heat is from a renewable source and can be applied for a long duration for low cost. The experimental approach used in this study involves column tests in which a vacuum is used to draw air through an unsaturated soil column contaminated with diesel fuel at residual saturation. Three tests were performed in which the soil column was heated to different temperatures and a vacuum was imposed to result in a constant upward air flow rate through the soil column. The data collected, including the air flow rates, the soil temperature and dielectric permittivity, and the total petroleum hydrocarbon in the gas phase at different locations, indicates that moderate increases in temperature lead to small increases in the removal of diesel from the unsaturated soil layer. However, the increases observed in the amount removed did not lead to a significant change in the percent of initial diesel removed. These results confirm that moderate increase in temperature are not sufficient to significantly improve diesel remediation from a low-permeability silt. However, it does demonstrate a potential for integrating SBTES systems with subsurface remediation strategies for more volatile contaminants to provide a sustainable approach for the reuse of contaminated sites.

Acknowledgements

The author wishes to thank her advisor, Professor John Scott McCartney, for facilitating this research opportunity. Special recognition is given the members of the thesis committee: Professors Dobroslav Znidarčić and Angela Bielefeldt. The advice of these three professors, given in times of difficulty, has been indispensable to this research. A special thank you is offered to the CEAE department for allowing access to laboratory materials and equipment. Another special thank you is offered to the many geotechnical graduate students and post doctorates who helped keep this project moving forward by sharing their expertise, knowledge, and enthusiasm especially James Rosenblum, Hanna Iezzoni, David Provost, and CJ Coccia. Most importantly the author extends her infinite gratitude to her incredibly supportive family and friends. This includes, but is not limited to, her parents, sister, Barrett Sather and her pup Lily. Financial support from the University of Colorado Innovative Seed Grant program and the Sustainable Energy Pathways grant received from the National Science Foundation (CMMI 1230237) is greatly appreciated.

Contents

Chapter

Tables

Table

Figures

Figure

Chapter 1

Introduction

1.1 Motivation and Problem Statement

Many cities are encouraging reurbanization to stimulate economic revitalization in inner-city areas. Unfortunately, the subsurface in urban areas is often contaminated with non-aqueous phase liquids (NAPLs) from historic industrial activities or leaking underground storage tanks. Although redevelopment of such brownfield sites poses a significant economic incentive for investors, in many cases the contaminant concentrations are high enough that an active remediation approach is needed to eliminate threats to groundwater. This is the case for sites contaminated with relatively light, organic NAPLs that are found in gasoline and diesel fuel that are present in the vadose zone or atop the water table. For sites with a deep water table, the most common remediation approaches are bioremediation and soil-vapor extraction (SVE). Bioremediation is usually the less expensive alternative, but can take years to complete. A moderate increase in temperature may enhance both the SVE process as well as bioremediation processes, potentially decreasing the required time and energy needed for remediation. Unfortunately, many engineers may avoid thermal processes due to prohibitive costs, or seek to raise the temperature to very high levels (300-400 °C) in an effort for quick results. Although very high temperatures may enhance the SVE process, they will inhibit most naturally occurring bioremediation processes. A potential opportunity to reduce the cost of supplying heat to the subsurface may be to combine the soil remediation process with heat collected from Soil-Borehole Thermal Energy Storage (SBTES) systems. SBTES systems involve the storage of thermal energy from renewable sources (solar thermal panels) within an array of closed-loop

borehole heat exchangers in the subsurface to provide heating for buildings in the winter. SBTES systems in the vadose zone involve both a vapor barrier at the soil surface as well as an insulation layer to trap the heat, as shown in (Fig. 1.1). Using SBTES for thermally-enhanced bioremediation and SVE may reduce remediation costs and lead to useful, long-term heat storage, revolutionizing the redevelopment of brownfield sites. As this is a preliminary study, the experimental approach is focused on thermally-enhanced SVE, and thermally-enhanced bioremediation is left for a future study.

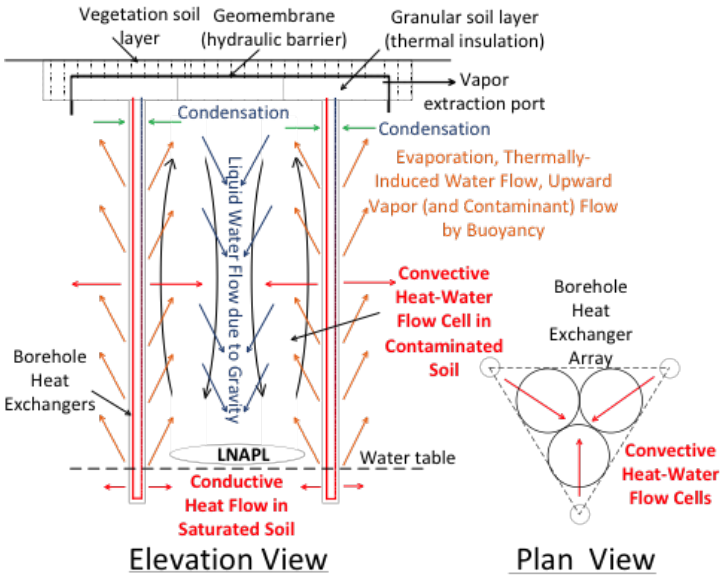

Figure 1.1: SBTES system in the vadose zone used for thermally-enhanced site remediation. Adapted from McCartney et al. (2013).

1.2 Hypothesis

The hypothesis of this research is that the temperature range in SBTES systems (40 to 60 °C) is sufficient to lead to an increase in the vapor pressure of the chemicals within the LNAPL (specifically diesel fuel) and water. Advective airflow through the soil generated by a soil vapor extraction system, will then carry the water and vapor-phase LNAPL through the soil layer to be extracted at the surface. It is a well known fact that the vapor pressure of LNAPLs increases significantly with temperature (Wilhoit and Zwolinski 1971). An increased vapor pressure signifies

that more of the LNAPL will be in the vapor phase. As air from areas outside of the contaminated zone, enters the contaminated soil it will become partially saturated with LNAPL. The flowing gas will then transport the vapor-form LNAPL out of the soil layer. The saturated vapor pressure for LNAPL in air also increases with temperature (Wilhoit and Zwolinski 1971). An Increase in temperature may also dry out the soil decreasing the degree of water saturation and increasing the air relative permeability. This will allow more air to flow through the soil increasing the amount of LNAPL extracted.

1.3 Research Objectives

The research objectives of this study are to:

(1) Characterize the flow processes and contaminant transport in a soil vapor extraction system

   (a) Define the factors that affect volatilization of LNAPL mixtures in unsaturated soil

   (b) Understand the transport of vapor water and vapor LNAPL mixtures in unsaturated soil layers during advective air flow

(2) Understand the effects of temperature on the flow processes and contaminant transport in a soil vapor extraction system

   (a) Temperature effects on the chemical properties of the individual LNAPL components independently and as a mixture.

   (b) Temperature effects on the degree of water saturation and how this will affect relative air permeability in a low permeability compacted silt.

   (c) Temperature effects on advective airflow.

(3) Characterize how small increases in soil temperature will affect contaminant removal in a SVE system.

1.4 Approach

An experimental approach is used to characterize the coupled flow of heat, water and LNAPL in unsaturated soil layers, leading to a better understanding of their effects on contaminant removal in thermally enhanced soil vapor extraction. Specifically, an insulated, cylindrical column will be filled with an unsaturated soil layer that has been uniformly mixed with diesel hydrocarbon before compaction, underlain by a vapor diffusion layer. The materials were carefully selected. The artificially-contaminated soil chosen was a low-permeability silt. The contaminant was diesel fuel obtained at a local gas station. Diesel was chosen because it is made up of semi-volatile hydrocarbons. This was important so that only a small fraction of the contaminant would be lost while mixing the contaminant with the soil and so that the SVE process would not happen too quickly in the experiment. After heating the soil column from the boundary, a vacuum is applied to the top of the soil column to induce soil vapor extraction. Dielectric sensors are used to measure the dielectric permittivity and temperature of the soil at different depths, which can be used to characterize the flow processes for heat and water. Gas sampling needles are inserted into the soil layer to measure changes in the vapor-phase LNAPL concentration as a function of space and time using gas chromatography. The vapor-phase LNAPL concentration in the effluent gas extracted from the top of the soil column is also tracked as a function of time. The instrumentation incorporated into the system is sufficient to characterize the flow process and the contaminate removal process under non isothermal conditions.

1.5 Scope

Chapter 2 includes a conceptual background explaining the fate on LNAPLs in the environment and a basic description of SVE. Chapter 3 presents the theoretical understanding of compressible flow and multicomponent transport. A review of previous studies is given in Chapter 4. A summary of the properties of the materials used in this study is given in Chapter 5, followed by an overview of the experimental setup in Chapter 6. Chapter 7 contains a detailed description of

the experimental procedure used. The results and analysis of this study are presented in Chapter 8 and Chapter 9, respectively. Lastly, Chapter 10 contains the conclusions.

Chapter 2

Conceptual Background

2.1 Fate of LNAPLs in the Environment

Nonaqueous phase liquids (NAPLs) are often introduced to the subsurface via leaking underground storage tanks, illegal and legal industrial disposal, and overland transportation accidents including pipeline and transportation trucks (Rothenstein 2003). Since this study uses diesel fuel as the contaminant, the following discussion is restricted to the fate of light nonaqueous phase liquids (LNAPLs) in the environment. Once the LNAPL mixture has entered the subsurface, the free phase LNAPL will begin to flow downward under the pull of gravity, through the vadose zone, while the most volatile components will begin to volatilize and release into the atmosphere. As the free phase LNAPL flows downward, some will be trapped in the pores due to capillary forces and immobilized at residual saturation.

The free phase LNAPL will continue flowing downward until it reaches the groundwater table. The amount of LNAPL that reaches the groundwater is dependent on the volume spilled and the depth of the water table. The amount of LNAPL trapped in the vadose zone is higher for sites with deep groundwater tables. Since LNAPLs are less dense than water, the LNAPL mixture that reaches the groundwater will pool on top of the water table. The pooled LNAPL will begin to move laterally over the groundwater table via capillary spreading. This lateral movement of the free phase LNAPL on top of the water table can be with or against the groundwater gradient. Hinchee and Reisinger (1985) report data from a field site that suggests diffusive transport can also play a role in spreading the contaminant from the LNAPL pool and contaminating groundwater

much further than just capillary spreading. The free-phase LNAPL transport rate and spreading of the contaminant plume generally depends on the bulk properties of the LNAPL mixture: density, viscosity, and hydrophobicity. It also depends on the properties of the porous media matrix (USEPA 1996). Some of the layer of floating free-phase contaminant will dissolve into pore water. The amount dissolved into the pore water depends on the aqueous solubility of each constituent in the contaminant mixture and the constituent's mole fraction of the mixture (Mercer and Cohen 1990). The free phase LNAPL that makes it to the groundwater can also become trapped at residual saturation inside the saturated zone. Wilson et al. (1990) observed residual saturation levels in the saturated zone that ranged from 14% to 30% in unconsolidated sands.

There are multiple techniques available that are able to remove the layer of floating free-phase LNAPL. Two common examples given are skimming systems and free product recovery with water table depression. Although these methods work well for removing the pooled LNAPL, some residual amount of LNAPL will remain in the vadose zone. For a medium sand, only a portion (around 50%) of the free phase LNAPL is actually recoverable using the pump and treat approach (USEPA 1996). The rest of the remaining LNAPL is being held in the pores at residual saturation levels by capillary forces. The relationship between the capillary pressure (the difference between the pressures in the non-wetting and wetting fluid phases in a soil) and the amount of LNAPL in the soil is referred to as the capillary pressure curve. An example for a two phase system with trichloroethylene (TCE) as the wetting phase and air as the non-wetting phase is shown in Figure 2.1. This figure indicates that after a certain capillary pressure is applied, very little change in TCE saturation will occur with further changes in capillary pressure, which corresponds to the point of residual saturation.

The amount of LNAPL that remains in the vadose zone at residual saturation levels depends on the porous media, contaminant type and volumetric water content. Hoag and Marley (1986) performed experiments measuring the residual saturation capacity of different soils to gasoline. They reported an average residual saturation at field moisture conditions of 16% for medium sands and 20% for fine sands. Baehr (1987) notes that even years after the initial contaminant release,

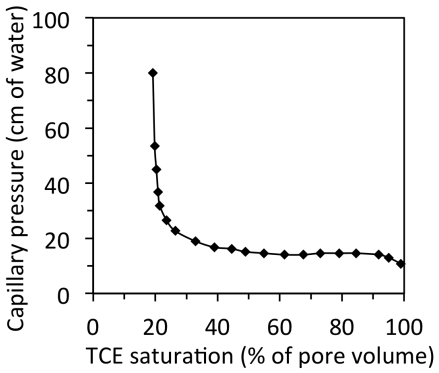

Figure 2.1: Experimentally derived capillary-pressure curves for trichloroethylene and air in fine sand. Adapted from Fetter (1999).

the amount of total petroleum hydrocarbons (TPH) dissolved in the pore water is still a significant percentage of predicted maximum levels. The LNAPL components dissolved in the pore water may leach from the soils for long periods of time and travel extensive distances (Marley and Hoag 1984). According to the EPA a very small quantity of petroleum hydrocarbons can contaminate a significant amount of groundwater (USEPA 1996). This implies that LNAPLs held at residual saturation levels can be a source of long term groundwater contamination and that remediation of residual LNAPL from the unsaturated zone is necessary to protect the groundwater supply.

2.2 Soil Vapor Extraction

In the past, the traditional remediation strategy for contamination at residual saturation levels was excavation. However, in the last few decades the SVE remediation method has become more popular. Excavation and disposal is very expensive and cannot be performed in areas with preexisting infrastructure. Soil vapor extraction (SVE) is a very popular, effective and economical in situ remediation method for vadose zone contamination (Marley and Hoag 1984). SVE creates an advective airflow through the contaminated porous media inducing volatilization and vapor transport of the contaminant. The SVE system consists of a vertical (or sometimes horizontal) vadose zone extraction well (or wells) connected to a vacuum pump at the surface, as shown in Figure 2.2. The wells are slotted through the contaminated zone. The pressure differential

created by the vacuum pump induces horizontal airflow through the soil, inducing transfer of the contaminant to the air stream. The volatilized contaminant is then extracted through the well and either released into the atmosphere or treated depending on local environmental regulations. The literature suggests that one pore volume of soil vapor should be extracted at least daily for effective remedial progress (USEPA 2004). To increase efficiency and to better direct the flow through the contaminated zone, air inlet wells can be placed surrounding the extraction well.

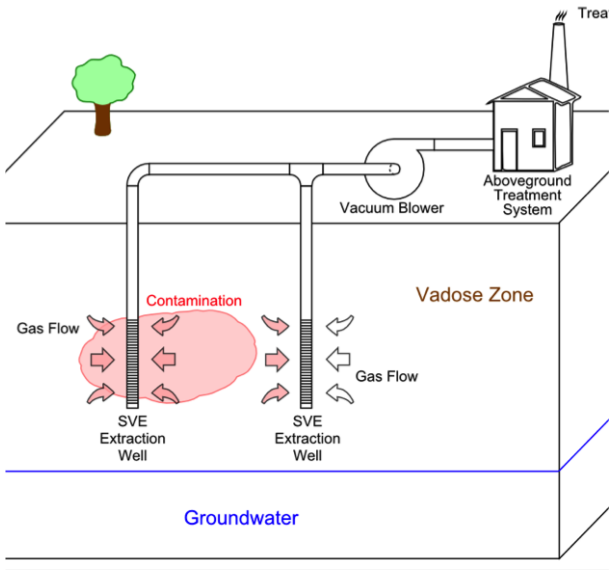

Figure 2.2: Simple schematic of a traditional SVE system

Thermally enhanced soil vapor extraction (TESVE) combines conventional SVE with heating the ground in situ in an effort to increase contaminant removal from the ground. There are many ways to heat the soil. Some of the most common heating processes are electrical resistance, electromagnetic heating, radio frequency heating, and hot-air injection. All of the above heating processes require a large amount of energy to operate and are usually very expensive. This study proposes using the heat collected from soil-borehole thermal energy storage (SBTES) systems as an alternative to conventional heating methods. SBTES systems consist of an array of closely spaced vertical geothermal boreholes and are used for storing heat collected from solar thermal panels. The temperature of the soil in these systems is expected to reach values ranging from 40 to 60 °C.

The actual ground temperature will depend on both the borehole spacing as well as the solar heat flux and heat transfer rate (Baser et al. 2015). A typical heat transfer rate for a SBTES system is 35 W per meter of heat exchanger in the ground. The number of solar thermal panels required depends on the length of heat exchangers and the heat transfer per panel.

The thermal properties of the unsaturated soil also affect the function of SBTES systems (Baser and McCartney 2015). Soil thermal properties are strongly influenced by the volume of water, air and solids in the soil. The specific heat of a soil is the amount of heat per unit mass required to raise the temperature of the soil by one degree Celsius. The specific heat of a soil depends on the composition of the solids and the amount of water. It typically ranges from 800 to 1480 J/(kg×K). Another thermal property of soils is thermal conductivity. The thermal conductivity of a soil describes its ability to transfer heat. The thermal conductivity of water, dry air, and quartz mineral are typically 0.58 (at 20C), 0.024 (at 20C), and 6.15-11.3 W/mK respectively. Because soil is a mixture of all three, the thermal conductivity of unsaturated soil is a function of water and air content. The thermal conductivity of soil also varies with temperature (Traore 2013). For a SBTES system, the specific heat and thermal conductivity of the soil will affect the amount of input energy required to maintain a given ground temperature, as well as the amount of heat that can be extracted from the system.

Although, the ground temperature in SBTES systems are significantly lower than those usually found in conventional TESVE, the thermal energy injected into the SBTES system is obtained freely from a renewable source. To understand how moderate increases in ground temperature will affect SVE, one must understand how temperature affects the physical processes that control the volatilization and movement of LNAPLs. The success of SVE depends on the ability to produce volatilization of the trapped contaminant and a steady airflow through the contaminated porous media to transport the volatilized contaminant to the surface.

Chapter 3

Theoretical Background

3.1 Overview

In general, an unsaturated soil layer contaminated with light non aqueous phase liquids (LNAPLs) must be treated as a multiphase system. Assuming a non-deformable and static porous media, flow can potentially occur in the gas, water and immiscible LNAPL fluid phase. In this three-phase system, water is considered the wetting phase while both air and LNAPL are the nonwetting phases. In situations where soil vapor extraction (SVE) is applicable, the contaminant is assumed to have thoroughly drained by gravity through the unsaturated zone, the contaminant is at residual levels and immobilized by capillary forces, the system can be simplified by assuming the LNAPL is immobile. This assumes that the LNAPL-air capillary forces are strong enough that momentum transfer from the mobile gas phase is not an issue (Rathfelder et al. 1991). The problem is then reduced to simultaneous flow of two immiscible fluids (air-water). Depending on how close the volumetric water content of the system is to residual saturation for water, the system can be simplified even further by assuming the water-phase is also immobile. This is a good assumption in many situations depending on how far your zone of contamination is above the water table and the shape of the soil water retention curve (SWRC). Some example SWRCs for different soils are given in Figure 3.1.

For sites with relatively deep water tables, immobilized water is usually a good assumption for most types of soils. The rest of this study will assume the water-phase is immobile, as the focus is on removal of contaminants after residual saturation has been reached. The discussion

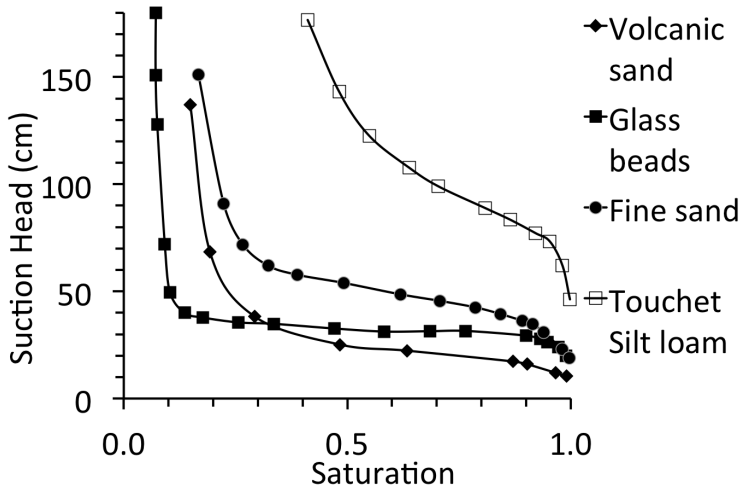

Figure 3.1: Suction head as a function of saturation for porous materials of varying pore-size distributions. Adapted from Brooks and Corey (1964).

below provides the theoretical framework for analysis related to thermally induced SVE (SVE). The analysis includes compressible gas flow and multicomponent mass transport in a multiphase porous medium. The gas flow discussion includes the effect of temperature on gas compressibility and fluid properties. The multicomponent mass transport assumes local equilibrium conditions for partitioning between phases.

3.2 Compressible Fluid Flow in Unsaturated Porous Media

As mentioned above, SVE is applicable in the unsaturated zone where water and LNAPL are immobile and the saturation of LNAPL is at residual saturations. Thus the only mobile fluid in the porous media is air. The governing equation for transient single-phase compressible fluid flow presented in Bear (1972) is given as:

$$\frac{\partial}{\partial t}(\rho_g \phi_g) + \nabla \cdot (\rho_g \mathbf{q}_g) = 0 \tag{3.1}$$

where ρ_g is the temperature and pressure-dependent density of the gas, ϕ_g is the gas phase porosity of the porous media, and $\mathbf{q}_g$ is the specific discharge rate of the gas. The gas phase porosity is

defined as:

$$\phi_g = S_g n \tag{3.2}$$

where S_g is the saturation of the gas phase and n is the porosity of the porous media. Assuming the porous media is not deformable, n can be considered constant. By applying the ideal gas law, the density of the gas can be expressed in terms of pressure and temperature as:

$$\rho_g = \frac{M_g P}{RT} \tag{3.3}$$

where ρ_g is the density of the gas, M_g is the molecular mass of the gas, R is the ideal gas constant, and T is the temperature in Kelvin. The specific discharge is defined using Darcy's Law as follows (Bear 1972):

$$\mathbf{q} = -\frac{k k_r a}{\mu_g} \left[\nabla (P + \rho g z)\right] \tag{3.4}$$

where k is the intrinsic permeability which is a property of the pore geometry, structure and connectivity of the porous media, k_{ra} is the permeability of the gas phase, μ_g is the viscosity of the gas; and z is the elevation. Combining Equations 3.1 through 3.4, the equation for single-phase compressible flow can be rewritten as:

$$n \frac{\partial}{\partial t} \left[S_g \left(\frac{M_g P}{RT} \right) \right] = \nabla \cdot \left[\left(\frac{M_g P}{RT} \right) \frac{k k_r a}{\mu} \left(\nabla P + \left(\frac{M_g P}{RT} \right) g \mathbf{k} \right) \right] \tag{3.5}$$

Assuming temperature is constant, gravity driven flow can be neglected and the term on the right drops out, simplifying the equation to:

$$n \frac{\partial}{\partial t} \left[S_g \left(\frac{M_g P}{RT} \right) \right] = \nabla \cdot \left[\left(\frac{M_g P}{RT} \right) \left(\frac{k k_r a}{\mu} \nabla \mathbf{P} \right) \right] \tag{3.6}$$

To fully describe the gas flow in a SVE system Equation 3.6 must be combined with interphase mass transfer terms, represented by I_{wg} and I_{Lg}. The terms, respectively, describe the transfer of mass from the water and LNAPL phases to the gas phase. The complete equation describing the single-phase gas phase flow in a SVE system where the water and LNAPL are considered immobile and the temperature is constant is expressed as:

$$n\frac{\partial}{\partial t}\left[S_g\left(\frac{M_g P}{RT}\right)\right] = \nabla\cdot\left[\left(\frac{M_g P}{RT}\right)\left(\frac{kk_r a}{\mu}\nabla\mathbf{P}\right)\right] + I_{wg} + I_{Lg} \tag{3.7}$$

3.2.1 The Slip Phenomenon: Klinkenberg Effect:

The above equation assumes Darcy's Law is valid for gas flow in soils. Although this may be true in many cases, authors have observed at low pressure that in certain kinds of soils air permeability is much higher than hydraulic permeability for the same porous medium. This is because in certain situations gas flow behaves differently than liquid fluid flow and achieves velocities higher than those produced by Darcy's law. This is because Darcy's law, which is based on the assumption of laminar flow, assumes no slip flow (i.e. zero velocity) on the contact surface between the fluid and porous media. When the diameter of the pore throat becomes small enough, this assumption is no longer valid for gas flow. The gas begins to slip over the walls of soil particles, thus obtaining a nonzero velocity at the contact. This nonzero velocity adds an additional flux to the flow. Thus in soils where this Klinkenberg effect occurs, the air permeability will be higher than what is predicted using Darcy's Law. The following equation, developed by Klinkenberg (1941) and summarized by (Bear 1972), is used to correct for the increased permeability:

$$k_g = k_l\left(1 + \frac{4c\lambda}{r}\right) = k_l\left(1 + \frac{b}{P}\right) \tag{3.8}$$

where k_g is the gas permeability, k_l is the liquid permeability, λ is the mean free path of the gas molecules under the mean pressure P at which k_g is determined, c is a proportionality factor, r is the radius of the capillary tube or pore throat size, and b is a constant for a gas-solid system that depends on the free path of the gas and the size of the openings in the porous media (Bear 1972). Corey (1986) observed that the Klinkenberg effect for coarse sands is usually small but can be very substantial in silt and clays. As silt is used in this study, the Klinkenberg effect could be important to consider.

3.3 Multicomponent Mass Transport

The LNAPL mixture trapped in the unsaturated zone can theoretically partition into the pore gas via all three of the other phases: LNAPL, water, and solid phase. In general, it is assumed that the pore matrix is completely water-wet and thus the direct transfer from solid to gas is not possible, but must first pass through the pore water. This assumption is assumed in the subsequent discussion. The rate at which this partitioning can occur depends on the chemical properties of each component in the mixture. Rathfelder et al. (1991) presents mass balance equations describing each γ component of the LNAPL mixture in each of the four α-fluid phases (gas (g), water(w), LNAPL (L), solid (s)):

$$\frac{\partial}{\partial t}(C_{w\gamma} n S_w) = I^{\gamma}_{w\beta} \tag{3.9}$$

$$\frac{\partial}{\partial t}(C_{L\gamma} n S_L) = I^{\gamma}_{L\beta} \tag{3.10}$$

$$\frac{\partial}{\partial t}(C_{g\gamma} n S_g) + \nabla \cdot n S_g (C_{g\gamma} \mathbf{V}_{mg} + \mathbf{J}_{g\gamma}) = I^{\gamma}_{g\beta} \tag{3.11}$$

$$\frac{\partial}{\partial t}(C_{n\gamma} \rho_s) = I^{\gamma}_{s\beta} \tag{3.12}$$

where $C_{\alpha\gamma}$ is the concentration of the γ-component in the α phase, S_alpha is the α-phase saturation, n is the porosity of the porous media, and ρ_s is the bulk density of the solids. $I^{\gamma}_{\alpha\beta}$ is the net rate of mass transfer of the γ-component to the α-phase from all the other adjacent phases. The variables $C_{g\gamma}\mathbf{V}_{m\gamma}$ and $\mathbf{J}_{g\gamma}$ are the γ-component mass fluxes in the α-phase by advection and dispersion, respectively. There are no source or sink terms in the mass balance equations above. Organic contaminants such as LNAPLs can undergo chemical or biological transformations that can either reduce or transform the composition of the LNAPL. Such transformations are complex and difficult to predict, so they are neglected in this study. Summing the Equations 3.9 to 3.12 over the four phases, the governing equation for the advective-dispersion mass transport of the γ component of the LNAPL mixture can be written as:

$$\frac{\partial}{\partial t}(C_{w\gamma} n S_w + C_{L\gamma} n S_L + C_{g\gamma} n S_g + C_{s\gamma} \rho_s) + \nabla \cdot n S_g (C_{g\gamma} \mathbf{V}_{mg} + \mathbf{J}_{g\gamma}) = 0 \tag{3.13}$$

The interphase mass transfer terms do not appear in Equation 3.13 because when they are summed over all the phases, the net interphase mass transfer is zero.

3.3.1 Advective Flux

As mentioned above, the gas phase is considered the only mobile phase. Given the high flow rates used in SVE, the gas-phase pressure is assumed to be controlled by the externally applied stress from the vacuum generating the airflow through the soil. The vapor-phase specific discharge of the γ-component is defined using Darcy's Law, neglecting gravity in the definition of the gradient due to the negligible weight of the vapor phase, and is given below:

$$nS_g\mathbf{V}_{mg} = -\frac{kk_ra}{\mu_g}\nabla P \tag{3.14}$$

where k is the intrinsic permeability, k_{ra} is the permeability of the gas phase, μ_g is the viscosity of the gas. As mentioned above, for low permeability soils the Klinkenberg effect may need to be considered when calculating the relative permeability.

3.3.2 Dispersive Flux

In this discussion, dispersion is only considered significant in the gas-phase, and neglected in the water and LNAPL-phases. Fick's Law is used to calculate a dispersion tensor that takes into account the combined processes of kinematic dispersion and molecular diffusion, as shown below:

$$\mathbf{J}_{g\gamma} = -D_{g\gamma}\nabla\ C_{g\gamma} \tag{3.15}$$

Substituting the advective and dispersive fluxes into Equation 3.13, the γ-component mass transport equation can be written as:

$$\frac{\partial}{\partial t}(C_{w\gamma}nS_w + C_{L\gamma}nS_L + C_{g\gamma}nS_g + C_{s\gamma}\rho_s) = \nabla \cdot nS_g(C_{g\gamma}\frac{kk_ra}{\mu_g}\nabla P + D_{g\gamma}\nabla\ C_{g\gamma}) \tag{3.16}$$

3.4 Interphase Mass Transfer: Equilibrium Partition Coefficients

Because SVE depends on the transfer of the LNAPL mixture components in the LNAPL, water and soil-phases to the gas phase, the role of interphase mass transfer is very important in the rate of contaminant removal. The following discussion assumes the local equilibrium condition for contaminant partitioning between phases. The equilibrium partition coefficient between two phases is calculated as the ratio of the concentrations of the γ-component in one fluid over the other.

3.4.0.1 Air-LNAPL Mass Transfer

Raoult's Law (Eq. 3.17) and the ideal gas law (Eq. 3.3) are used to calculate the equilibrium coefficient for air and LNAPL. Raoult's Law states that the partial vapor pressure of each component i of an ideal mixture of liquids is equal to the vapor pressure of the pure component multiplied by its mole fraction in the mixture).

$$P_i = P_i^* * X_i \tag{3.17}$$

where P_i is the partial pressure of the component i, P_i^* is the pressure of component i in pure form, and X_i is the mole fraction of component i in mixture. The equation for an air-LNAPL partitioning coefficient for the γ-component of the LNAPL mixture is given below:

$$K_{gL}^{\gamma} = \frac{C_{g\gamma}}{C_{L\gamma}} = \frac{P_V^{\gamma}}{RT \sum_{\gamma=1}^{N} \frac{C_{L\gamma}}{M_{\gamma}}} \tag{3.18}$$

where P_V^{γ} is the γ-component vapor pressure at the system temperature, T, R is the universal gas constant, and M_{γ} is the molecular weight of the γ-component.

3.4.0.2 Air-Water Mass Transfer

Assuming local equilibrium conditions and LNAPLs of relatively low aqueous solubility, the air-water partitioning constant can be evaluated using the ideal gas law and Henry's Law. Henry's Law states that at a constant temperature, the amount of a given gas that dissolves in a given type

and volume of liquid is directly proportional to the partial pressure of that gas in equilibrium with the liquid (Eq: 3.19).

$$P = K_H * C \tag{3.19}$$

where P is the partial pressure of the gaseous solute above the solution, C is the concentration of the dissolved gas, and K_H is the Henry's law constant. The equation for air-water partitioning coefficient for the γ-component of the LNAPL mixture is written as follows:

$$K_{gw}^{\gamma} = \frac{C_{g\gamma}}{C_{w\gamma}} = \frac{M_{\gamma} K_h^{\gamma}}{RT} \tag{3.20}$$

where K_h^{γ} is the temperature dependent Henry's Law constant for the γ-component.

3.4.0.3 Water-LNAPL Mass Transfer

The octanol-water partition coefficient, K_{ow}, measures the ratio of the concentration of a chemical in octanol relative to the concentration of the chemical in water, when octanol and water-phases are at equilibrium (Eq. 3.21). K_{ow} can be used to estimate the water-LNAPL partition coefficient. The more hydrophobic γ-components will have larger values of K_{ow}.

$$K_{ow} = \frac{C_{\text{oct}}}{C_{\text{water}}} \tag{3.21}$$

3.4.0.4 Water-Solid Mass Transfer

Sorption of the LNAPL mixture by the solid particle of a soil matrix can limit the remediation potential by limiting the mass transfer of the LNAPL into the gas phase. Sorption is a real problem but is very complex and difficult to characterize. Organic carbon content of the soil, among many other factors, is known to increase the sorption potential of the soil. The soil used in this study has very low organic content so it is assumed that sorption is negligible. Substituting the above equilibrium coefficients: $K_{gw}^{\gamma} = \frac{C_{g\gamma}}{C_{w\gamma}}$ and $K_{gL}^{\gamma} = \frac{C_{g\gamma}}{C_{L\gamma}}$ into Equation 3.16 and assuming negligible adsorption, the γ-component equilibrium transport equation is given as:

$$[h]\frac{\partial}{\partial t}(\frac{C_{g\gamma}}{K_{gw}^{\gamma}}nS_w + \frac{C_{g\gamma}}{K_{gL}^{\gamma}}nS_L + C_{g\gamma}nS_g) = \nabla \cdot nS_g(C_{g\gamma}\frac{kk_r a}{\mu_g}\nabla P + D_{g\gamma}\nabla\ C_{g\gamma}) \tag{3.22}$$

Chapter 4

Literature Review

4.1 Overview

Conventional soil vapor extraction (SVE) has proven to be very effective in high permeable homogeneous soils contaminated with volatile organic compounds (VOCs) such as chlorinated solvents and lighter hydrocarbons in fuels such as gasoline. It is much less effective on semi-volatile organic compounds because their vapor pressures are too low at naturally occurring soil temperature. As mentioned, many of the equilibrium partitioning coefficients that control the concentration of the LNAPL phase in the gas phase depend on temperature. Theoretically, an increase in soil temperature could increase the range of compounds appropriate for SVE application to include semi-volatile contaminants, such as the heavier hydrocarbons found in diesel fuel.

4.2 Temperature Effect on Vapor Pressure

The most crucial factor affecting the success of SVE is the vapor pressure of the target contaminant. Vapor pressure is defined as the pressure exerted by a vapor in thermodynamic equilibrium with its liquid form at a given temperature in a closed system. Vapor pressure is strongly related to temperature. In general, vapor pressures of organic compounds increase by a factor of 3 or 4 with every 10 °C rise in temperature (Rathfelder et al. 1995). Antoine's Equation, shown in Equation 4.1, is one of the most commonly used equations to predict how vapor pressure changes with temperature.

$$P = \frac{1}{7.5} \times 10^{A - \frac{B}{C+T}} \tag{4.1}$$

Table 4.1: Normal alkane hydrocarbon vapor pressure predicted by Antoine's Equation in terms of temperature (Mackay et al. 1992a)

Hydrocarbon	Vapor Pressure (Pa)			
	20 °C	40 °C	60 °C	80 °C
C_8 n-Octane	1,885.18	4185.46	10558.25	23436.63
C_{10} n-Decane	174.73	477.17	1515.96	4071.71
C_{12} n-Dodecane	15.75	54.11	221.02	728.10
C_{14} n-Tetradecane	1.27	5.72	31.13	128.92
C_{16} n-Hexadecane	0.09	0.55	4.15	22.18

where A,B,C are compound specific constants, T is in °C and P is in Pascals. Table 4.1 lists some normal alkanes and their vapor pressures at different temperatures predicted using Antoine's Equation. Figure 4.2 gives a graphical representation of how vapor pressure changes with temperature. Field experience at conventional SVE sites indicate the recommended vapor pressure for compounds remediated by SVE is 70 Pa or above at 25 °C (Poppendieck et al. 1999a). Table 4.1 shows that many of the higher carbon number n-alkanes would not be suitable for conventional SVE. For example, n-Dodecane has a vapor pressure of 15.75 Pa at 20 °C and would not be suitable for conventional SVE. But, when the temperature increases to 60 °C, its vapor pressure increases to 221.02 Pa, theoretically making n-Dodecane suitable for thermally enhanced soil vapor extraction (TE-SVE).

Vapor pressure of a compound in a mixture also depends on the mole fraction of said compound in the mixture. This relationship is given by Raoult's Law (Eq. 3.17). As the LNAPL mixture changes composition the partial pressure of each component also changes. A component with a lower vapor pressure might not volatilize at significant quantities when it's mole fraction in the mixture is low. But as the more volatile components volatilize, the mole fraction of the less volatile components increases. This leads to an increase in partial vapor pressure, increasing its volatilization potential.

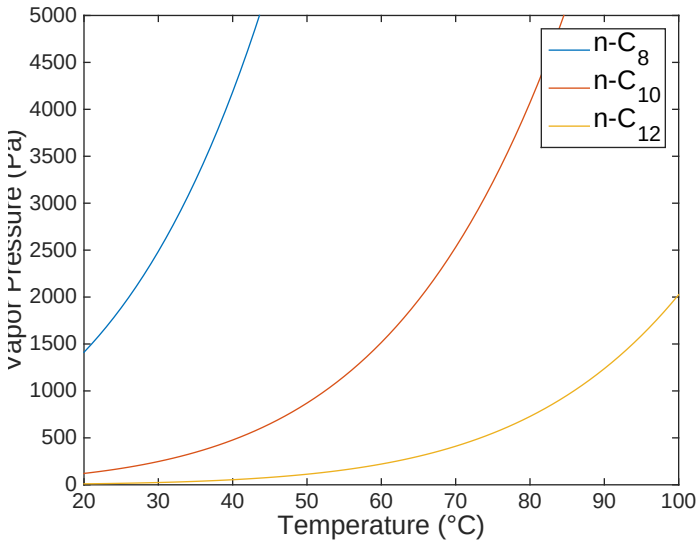

Figure 4.1: Vapor pressure with respect to temperature using Antoine's Equation

4.3 A Review of Past Studies on Thermally Enhanced Soil Vapor Extraction (TE-SVE)

One of the first experimental investigations into TE-SVE was performed by Oma and Buelt (1988). They performed two sets of experiments. The goal of the first set of experiments was to demonstrate how temperature effects the removal efficiency of different contaminants is different types of soils. The contaminates studied were 2-chlorophenol and hexaclorobenzene, whose physical properties are given in Table 4.2. The three soils tested are listed in Table 4.3.

Table 4.2: Physical properties of the contaminants tested by Oma and Buelt (1988)

Hydrocarbon	Molecular weight (g/mol)	Density (g/mL)	Melting point (°C)	Boiling point (°C)
2-chlorophenol	128.56	1.2632	9	175
Hexachlorobenzene	28.79	1.5691	230	322-326

Table 4.3: Soil mixture properties

Type of Soil	Gravimetric Water Content (%)	Chemical Concentration (wt%)
High-permeability Hanford sand	5.0	0.1
Ritzville silty loam	4.8	0.1
Low-permeability bentonite clay	55.4	0.1

The contaminated soil samples were heated to a 400 °C in an oven at a rate of 300 °C per hour. Their results are shown in Figure 4.2. It is clear that as temperature increased, the organic removal efficiency of each chemical in all three types of soils increased. The removal of 2-chlorophenol reached a higher efficiency than hexachlorobenezene, due to its differing physical properties. For both contaminants, a difference in efficiency between soil types is observed. Although, this effect decreases as the temperature increases.

The second set of experiments performed by Oma and Buelt (1988) compared static heating vs heating combined with a vacuum recovery system. These testes were performed using Hanford sand and 2-chlorophenol. Their results showed that by using a vacuum recovery system, 95% removal of the 2-chlorophenol was achieved, while only 70% removal occurred when no vacuum was used. Thus the combination of heat and a vacuum recovery system performed better at removing the contaminant than just heat alone.

Following the promising results proesented by Oma and Buelt (1988), researchers began experimenting with different types of in-situ heating techniques. Lingineni and Dhir (1992) performed thermal SVE column experiments where air, heated to a temperature of 80 °C, was introduced into columns filled with 360 μm-diameter glass beads contaminated with ethyl alcohol at residual saturation of 13%. The experiment relied on convective heat transfer from the air to heat the soil column. They saw that the contaminant evaporation process was increased in the vicinity close to the inlet but not for the soil further downstream. This was due to the fact that by the time the heated air was able to increase the temperature of the portions of the column further downstream, the contaminant had already been evaporated. Ethyl alcohol's vapor pressure is 5.95 kPa at 20 °C,

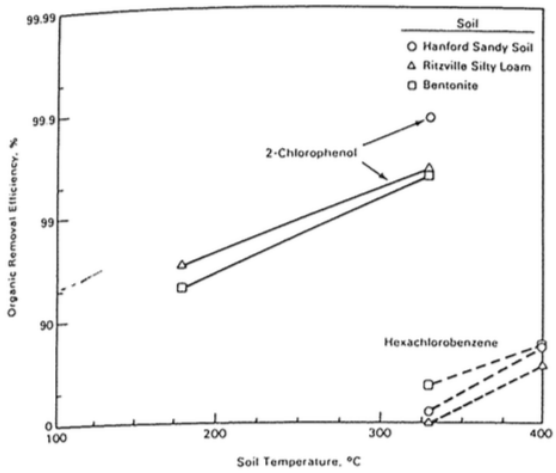

Figure 4.2: Organic removal efficiency as a function of soil temperature. Adapted from Oma and Buelt (1988)

making it quite volatile. Hence, for contaminants with high volatility TE-SVE using heated air is not practical. For less volatile contaminants, where the evaporation is slower, and the heated air has time to heat the soil upstream, enhancement of the evaporation process can be achieved. The results by Lingineni and Dhir (1992) reaffirm that an increase in temperature can be used to enhanced SVE for less volatile contaminants. It also showed that heating the soil via injection of heated air is very inefficient and slow.

Poppendieck et al. (1999a) investigated the relationship between temperature and hydrocarbon removal rates in an attempt to see if the increased cost of heating the soil is worth it in the field. They performed SVE column experiments at 50, 100, 125, and 150 °C on soil samples from a field site that was contaminated with diesel range organics (DRO). DRO includes hydrocarbons with 12 -20 carbons ($C_{12} - C_{20}$). In their experiments, they specifically tracked the straight chain alkanes $n - C_{13}$ through $n - C_{19}$. The hydrocarbon mass in the effluent of each hydrocarbon was recorded with time. Figure 4.3 and Figure 4.4 show the fraction of the compound remaining in the soil as a function of time at each temperature for tridecane (C_{13} and heptadecane C_{17}), respectively. The increase in temperature affected both the rate of compound removal from the soil and the fraction of the original compound mass remaining in the soil at the conclusion of the column study. For

the 50 °C test, this effect was greater for tridecane than heptadecane. For tridecane the fraction remaining in the soil was around 25% after 150 hrs. For heptadecane, the fraction remaining in the soil still remained very close to one after 150 hrs. Heptadecane requires the temperature to be increased to approximately 100 °C to create a substantial increase in removal efficiency.

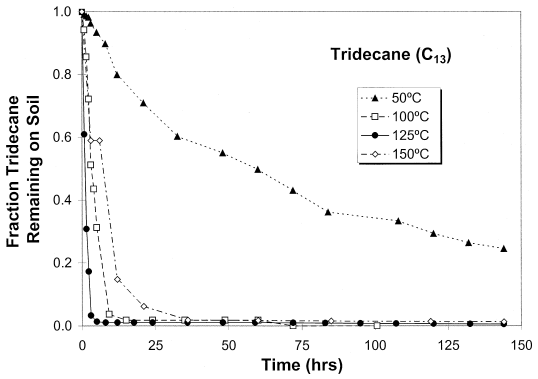

Figure 4.3: Fraction of tridecane (C_{13}) remaining in the soil as a function of time and temperature. Adapted from Poppendieck et al. (1999a)

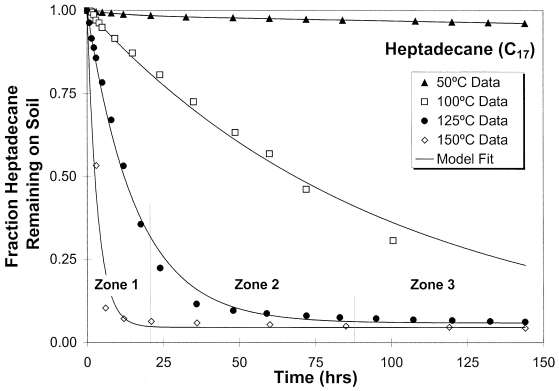

Figure 4.4: Fraction of Heptadecane (C_{17}) remaining in the soil as a function of time and temperature. Adapted from Poppendieck et al. (1999a)

Park et al. (2005) also studied the temperature dependent SVE removal rates of normal alkanes $n - C_{10}$, $n - C_{12}$, $n - C_{14}$ and $n - C_{16}$. They performed multiple SVE heated column experiments on soil with a porosity of 0.4, a dry density of 2500 kg/m^3 and a range of gravimetric water contents of 0-25%. The soil was contaminated with a mixture of the normal alkanes listed above at equal amounts by weight. Their first set of experiments were performed at temperatures of 60 °C and 100 °C for a constant flow rate of 40 mL/min. Figures 4.5 and 4.6 show the effluent hydrocarbon concentrations with respect to time, at temperatures of 60 and 100 °C, respectively. Their experimental data shows that compounds are removed by order of increasing volatility. This is the result of changes in the mole fraction of the hydrocarbon mixture. As the more volatile hydrocarbons are volatilized, the mole fraction of the less volatile hydrocarbons increases. According to Raoult's Law, as the mole fraction of less volatile hydrocarbons increases, their partial vapor pressures also increases. This increase in vapor pressure leads to an increases in their concentration

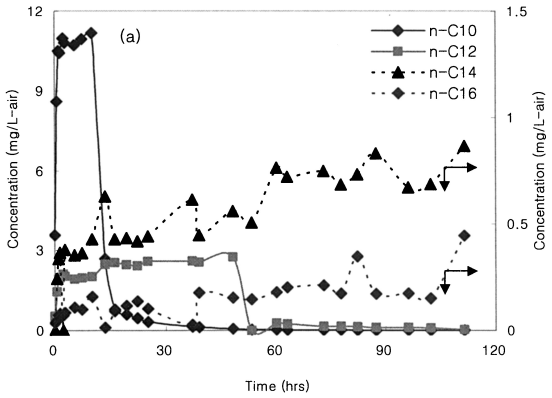

Figure 4.5: The gas phase concentration of n-alkanes with time at 60 °C. Adapted from Park et al. (2005)

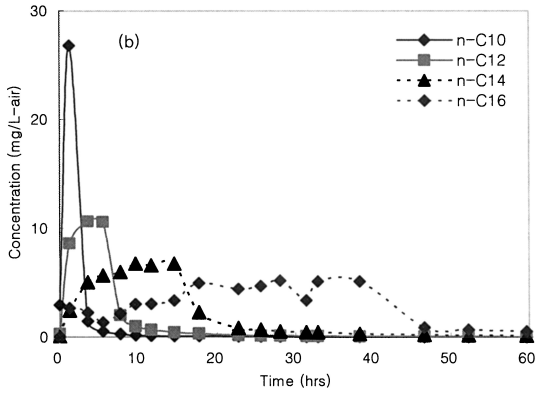

Figure 4.6: The gas phase concentration of n-alkanes with time at 100 °C. Adapted from Park et al. (2005)

in the effluent gas.

Park et al. (2005) also performed experiments to investigate the effect of airflow rate on the removal rates of n-alkanes. All experiments were conducted at a constant temperature of 100 °C with airflow rates ranging from 10 mL/min to 80 mL/min. The results for n-hexadecane (C_{16}) are given in Figure 4.7. If equilibrium partitioning between the free-phase LNAPL and gas phase is assumed, removal rates should increase as airflow rate increase. However, the results in Figure 4.7 shows this is not the case. The removal rate at 80mL/min is very similar to the removal rate at 40mL/min. This indicates the existence of rate-limiting mass transfer processes. This can be explained due to the fact that the contact time of the air with the contaminated soil decreases when the interstitial velocity of the air increases. When this contact time becomes too short equilibrium condition are not reached. To expand on this concept, Park et al. (2005) conducted experiments at varying flow rates for different temperatures. Their results showed that the effects of the rate-limiting mass transfer processes are decreased as temperature is increased. This signifies that equilibrium conditions can still be achieved at high flow rates as long as temperature is increased accordingly.

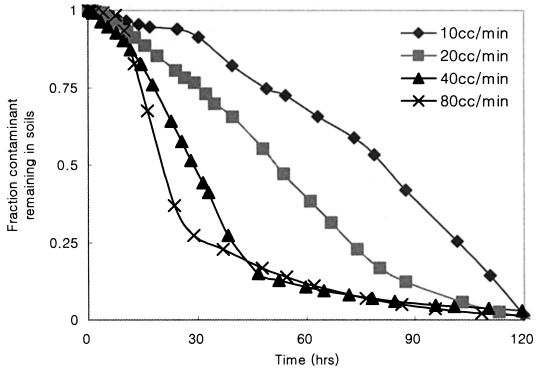

Figure 4.7: Effect of airflow rate on the removal of n-hexadecane (C_{16}) with time. Temperature was fixed at 100 °C. Adapted from Park et al. (2005)

Chapter 5

Materials

5.1 Overview

The physical modeling experiments in this study were performed on a layered column of soils compacted within a cylindrical column. A 70 mm-thick layer of sand was placed into the bottom of the column to act as a high permeability filter that would distribute gas uniformly. A 360 mm-thick layer of compacted silt that was mixed uniformly with diesel fuel was placed on top of the sand layer. The goal of the experiments was to evaluate the removal of the diesel from the compacted silt via thermally enhanced soil vapor extraction (SVE). The soil used in this study is a uniform quartz sand and a silt, obtained from a borrow source at the Bonny dam. The physical properties of sand, silt, and diesel fuel are presented below.

5.2 Sand

A coarse-grained sand was used in this study as a filter layer to redistribute the gas entering the bottom of the soil column. The grain size distribution of the sand is shown in Figure 5.1, and characteristic values from the curve are shown in Table 5.1. Based on these values, the sand is classified as SP according to the Unified Soil Classification System (USCS). The value of G_s was estimated to be 2.65. A 70mm-thick layer of sand was placed in dry conditions using tamping to reach a dry density of 1739 kg/m^3.

Table 5.1: Sand: Grain-size distribution values

Parameter	Value
D_{10}	0.9 mm
D_{30}	1.1 mm
D_{50}	1.35 mm
C_u	1.56
C_z	0.96
% Passing No. 200 Sieve	negligible

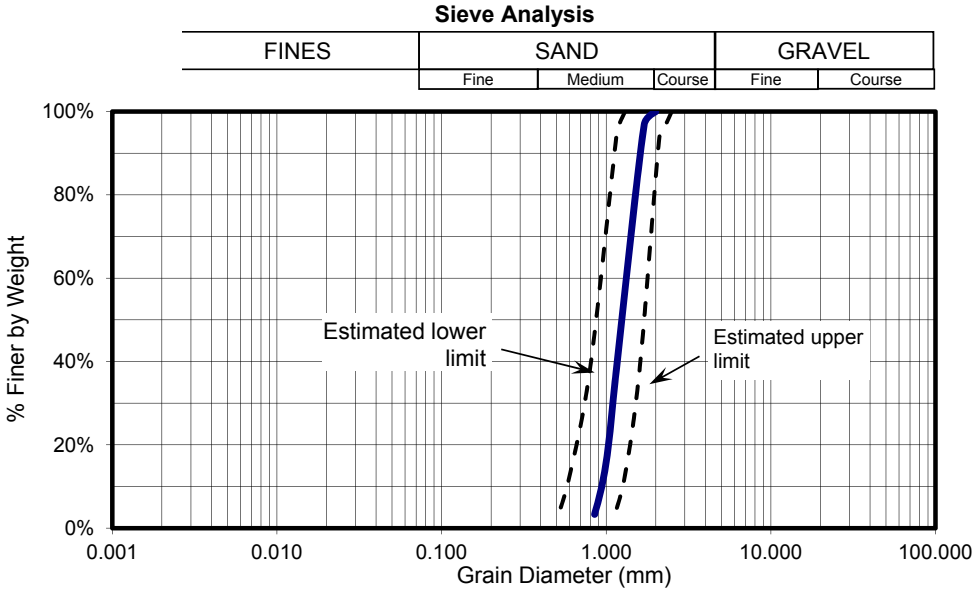

Figure 5.1: Sand: Grain-size distribution plot

5.3 Bonny Silt

A silt collected at the Bonny dam site in Yuma County located in eastern Colorado was used in this experiment as the unsaturated soil layer. The grain-size distribution curve of the Bonny silt is shown in Figure 5.2 and characteristic values from the distribution are summarized in Table 5.2. The specific gravity of a soil is defined as the mass of a certain volume of soil solids over the mass of the same volume of water at 20 °C. The average specific gravity (G_s) of the Bonny silt is 2.65. Atterberg limit tests were performed on the fines fraction of the soil. The liquid limit (LL) defines the water content where the behavior of a soil changes from a plastic to liquid. The plastic limit defines the water content were the soil's behavior begins to be plastic and the plasticity index is the difference between the liquid limit and the plastic limit. The Atterberg limits for the Bonny Silt are presented in Table 5.3. Based on these values and the grain size distribution, the soil is classified as ML according to the USCS. The fraction of organic carbon (F_{oc}) for Bonny silt is BLANK. The thermal conductivity of Bonnie silt depends on void ratio and ranges from 1.37 to 1.45 (W/(m×k)).

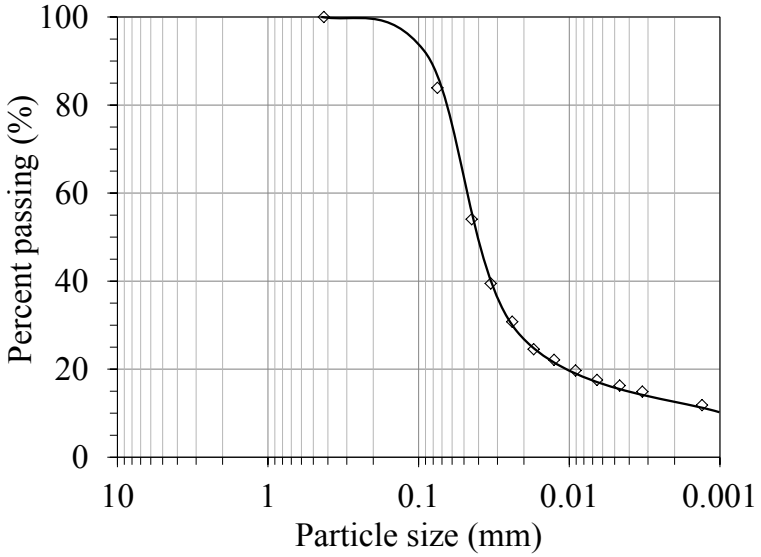

Figure 5.2: grain-size distribution plot for the Bonny silt

Table 5.2: Characteristic values from the grain size distribution for the Bonny silt

Parameter	Value
D_{10}	<0.0013 mm
D_{30}	0.022 mm
D_{50}	0.039 mm
% Passing No. 200 Sieve	83.9%
% Clay size	14.0%
% Silt size	69.9%
% Sand size	16.1%

Table 5.3: Atterberg limits for the Bonny silt

Parameter	Value
Liquid limit (LL)	24
Plastic limit (PL)	21
Plasticity index (PI)	4

The mass fraction of soil organic carbon content (F_{oc}) for Bonny silt is 0.0259. The thermal conductivity (k) of Bonnie silt depends on void ratio and ranges from 1.37 to 1.45 (W/(m×k)). The hydraulic conductivity of saturated Bonny silt ranges from 1×10^{-9} to 1×10^{-6} m/s for specimens having initial void ratios ranging from 0.5 to 0.9. In this study, the Bonny silt was compacted to an average void ratio of 0.89, a porosity of 0.47 and has an estimated saturated hydraulic conductivity of 1.3×10^{-6}. The intrinsic permeability is estimated to be 1.18×10^{-9} cm^2. According to the EPA, SVE is generally effective in soils with intrinsic permeability greater than or equal to 10^{-8} cm^2. For soils with intrinsic permeability between 10^{-8} and 10^{-10} cm^2, SVE may be effective depending on other factors (USEPA 2004).

5.4 Diesel Fuel

The diesel fuel used in this experiment was obtained at a local gas station. It is a light neon yellow in color with a strong "fuel" odor. Although the specific diesel fuel used in this study was not thoroughly characterized, the physical and chemical composition of a similar diesel fuel presented by in Zhendi (2003) is given in this section. Although no two diesel fuels are identical, the information below provides a general characterization of the diesel fuel used in this experiment.

A summary of some common physical properties of the example diesel fuel are listed in Table 5.4. The diesel fuel has a density of 0.8310 at 15 °C which is less dense than water, making it a LNAPL. As the table shows, The diesel fuel's density and viscosity both decrease as temperature increases. The surface tension of the diesel fuel with air and water at 0 °C and 15 °C are listed in Table 5.5. The multiphase flow of diesel fuel, air and water in porous media depends highly on the surface tensions between each of the fluids.

Table 5.4: Diesel fuel: summary of physical properties (Zhendi 2003)

Parameter	Value
Water Content	<0.1 (volume %)
Flash Point	54 °C
Density (0 °C)	0.8423 at 0 °C
Density (15 °C)	0.8310 at 15 °C
Dynamic Viscosity (0 °C)	4.08 (cP)
Dynamic Viscosity (15 °C)	2.76 (cP)

Table 5.5: Surface tension of diesel (Zhendi 2003)

Parameter	Value
Oil/Air Interfacial Tension (0 °C)	28.7 (mN/m)
Oil/Air Interfacial Tension (15 °C)	27.5 (mN/m)
Oil/Water Interfacial Tension (0 °C)	25.0 (mN/m)
Oil/Water Interfacial Tension (15 °C)	21.6 (mN/m)

Hydrocarbons are compounds composed of carbon and hydrogen. They are divided into two classes: aliphatic and aromatic compounds. Aliphatic hydrobcarbons can be either saturated or unsaturated. Saturated hydrocarbons (alkanes) are composed entirely of single bonds and are saturated with hydrogen. The general formula for saturated hydrocarbons is C_nH_{2n+2} and they can be either linear or branched. Saturated hydrocarbons are the basis of petroleum fuels. Aromatic hydrocarbon (Arenes) are hydrocarbons with alternating double and single bonds between carbon atoms forming rings. The simplest aromatic hydrocarbon is benzene. Aromatic hydrocarbons can be either monocyclic (MAH) or polycyclic (PAH). Table 5.6 lists the concentrations of saturated and aromatic hydrocarbons in the diesel fuel. As shown in Table 5.6, the saturated hydrocarbons

occur at a much higher concentration than the aromatic hydrocarbon.

Table 5.6: Hydrocarbon groups in diesel (Zhendi 2003)

Component	Concentration (weight %)
Saturates	88.2
Aromatics	10.2

Diesel fuel usually contains a large variety of hydrocarbons. Most GC methods are designed to measure the collective concentrations of extractable aliphatic and aromatic petroleum hydrocarbons. Extractable aliphatic hydrocarbons are collectively quantitated within two ranges: C_9 through C_{18} and C_{19} through C_{36}. C_n refers to a hydrocarbon with n carbons. Extractable aromatic hydrocarbons are collectively quantitated within the C_{11} through C_{22} range. These aliphatic and aromatic hydrocarbon ranges correspond to a boiling point range between approximately 150 and 265 °C. To give a general idea regarding the range of carbon numbers of the hydrocarbons in the diesel fuel, Table 5.7 gives the concentration in the diesel fuel fuel of each normal Alkane from C_8 through C_{28}. Alkanes with more than three carbon atoms can be arranged in various different ways, forming many structural isomers. A normal alkane is one in which the carbon atoms are arranged in a single chain with no branches For the diesel fuel the highest concentrations of normal alkanes are found between C_9 and C_{19}. In addition to the n-alkane concentrations in the diesel, Table 5.7 provides the boiling point, vapor pressure and solubility in water of a few of the n-alkanes listed.

Another group of specific hydrocarbons of interest is BTEX which includes benzene, toluene, ethylbenzene, and o-m-p xylenes. These compounds are some of the most volatile organic compounds (VOCs) found in diesel fuel. When assessing a site contaminated with diesel, the high volatility of BTEX makes it the easiest and quickest hydrocarbon group to test for. The presence of BTEX usually implies the existence of less volatile compounds and can aid in assessing the type of remediation required. Also Benzene is a known carcinogenic. The concentrations of BTEX for the diesel fuel are listed in Table 5.8.

Table 5.7: n-Alkane distribution of diesel (Zhendi 2003)

n-Alkane Component	Concentration (μg/g oil)	Boiling Point (°C)	Vapor Pressure (Pa @25 °C)	Solubility in water (mg/L @25 °C)
n-C8	1.15	126	1879.86	0.660
n-C9	4.24	151	593.29	0.220
n-C10	10.93	174	190.65	0.052
n-C11	13.43	195.9	54.93	0.044
n-C12	13.23	216	18.00	0.0037
n-C13	13.02	226	7.47	0.0047
n-C14	12.33	252	1.55	0.0022
n-C15	11.98	270	0.45	0.000076
n-C16	10.96			
n-C17	9.22			
n-C18	6.72			
n-C19	4.72			
n-C20	3.01			
n-C21	1.70			
n-C22	0.85			
n-C23	0.41			
n-C24	0.19			
n-C25	0.09			
n-C26	0.04			
n-C27	0.02			
n-C28	0.02			

Table 5.8: BTEX compounds in diesel (Zhendi 2003)

Component	Concentration (μg/g oil)
Benzene	136
Toluene	1024
Ethylbenzene	619
Xylenes	3774

Chapter 6

Experimental Setup

6.1 Overview

The experiment was conducted in a cylindrical acrylic container having an inner diameter of 228.6 mm and a height of 609.6 mm. A cross-section elevation view of the soil container for a typical setup is shown in Figure 6.1. The cylinder is enclosed on the top and bottom with large end caps that are fitted to the cylinder with o-rings to ensure an airtight seal. The end caps each have ports to which plumbing fittings can be connected. In the case of this experiment, the port in the bottom cap was used to supply air at atmospheric pressure to the bottom of the soil layer within the container, and the port on the top cap was used to supply vacuum to withdraw the contaminant from the soil using soil vapor extraction (SVE). Five dielectric sensors are placed throughout the center of soil column to record the variations of temperature and dielectric permittivity of the soil throughout the experiment. Due to a defective dielectric permittivity sensor on one the dielectric sensors, dielectric permittivity was only recorded in four locations. There are four vapor-sampling ports. One of the sampling ports was connected to the effluent line at the top of the container, and three were placed into the sidewall of the container at heights of 60, 180, and 300 mm above the base of the soil. The vapor sampling port on the effluent line is used to measure the vapor-phase total petroleum hydrocarbon (TPH) of the effluent gas and the three vapor sampling ports along the height of the soil column are used to measure the vapor-phase TPH concentration of the soil gas in the pore space throughout the experiment. The vapor-phase TPH concentrations of the gas samples were determined using a Gas Chromatographer (GC) equipped with a flame ionization

detector (FID). In the experiments involving elevated temperatures, , heating tape wrapped around the outside of the cylinder was used to heat the soil to the desired temperature. A schematic of the experimental setup is shown in Figure 6.2

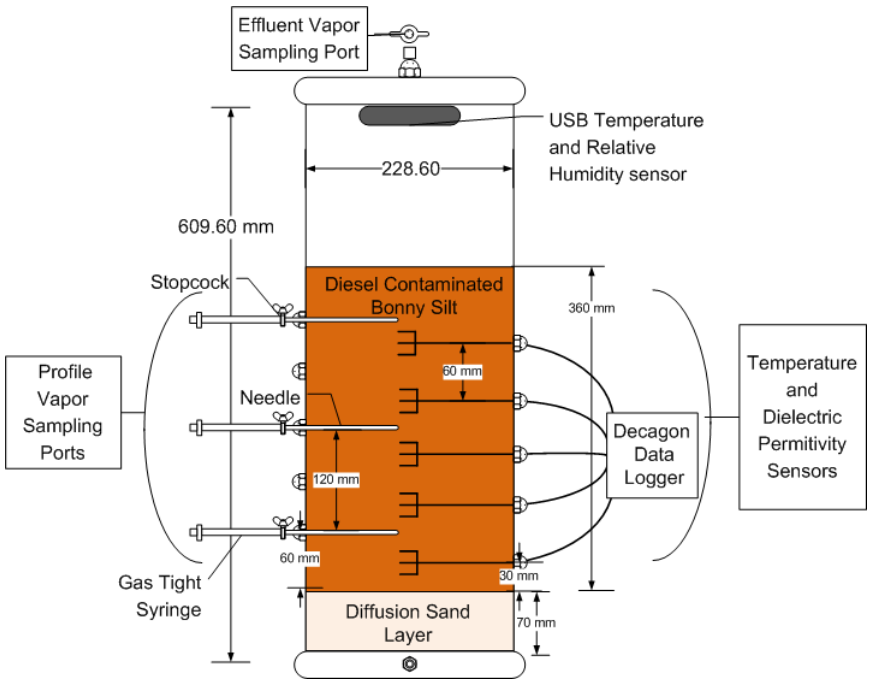

Figure 6.1: Cross-section elevation view of soil container for a typical setup

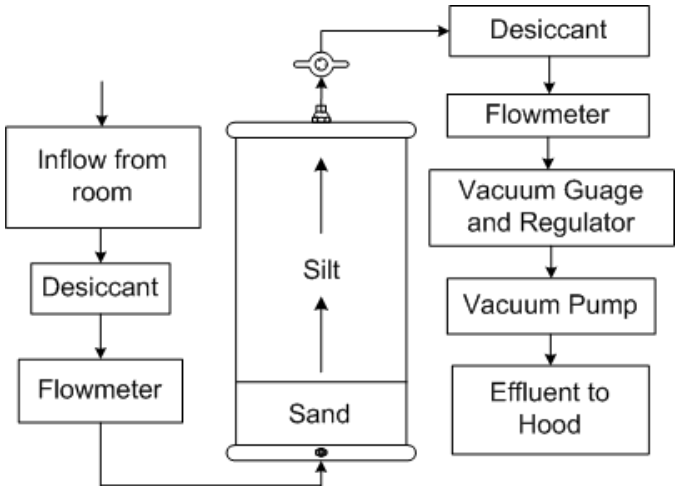

Figure 6.2: Schematic of overall experimental setup

6.2 Heating System

Heating tape was wrapped around the outside of the cylinder in order to heat the soil to the desired temperature during the thermal experiments as shown in Figure 6.3. Before placement of the tape, the cell was wrapped in aluminum foil. A temperature sensor was placed outside of the cell next to the heating tape to record the temperature of the heating tape. The whole cylinder was encased in fiberglass insulation to decrease the amount of heat loss as shown in Figure 6.4. The heating tape, as shown in Figure 6.5, was manufactured by HTS/Amptek Company. The heating tape was connected to a variable voltage meter, as shown in Figure 6.6, which was then plugged into an automatic timer.

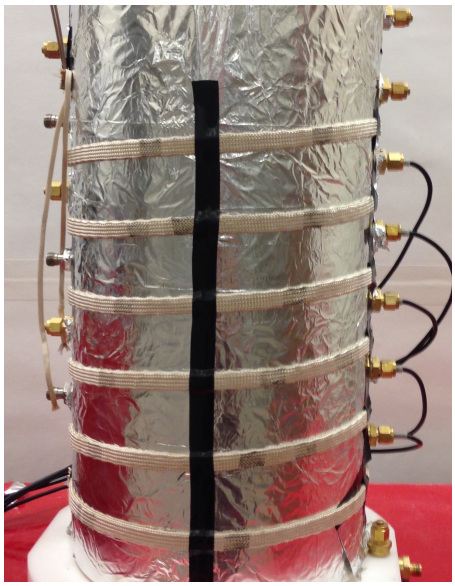

Figure 6.3: Heating tape wrapped around the cylinder

Figure 6.4: The cylinder was insulated with fiberglass

Figure 6.5: HTS/Amptek heating tape. The heating element is multi-strand resistance wire, braided with AMOX yarn and knitted into the serpentine shape.

Figure 6.6: Manual voltage regulator

Figure 6.7: Temperature sensor attached to the outside of the cylinder in order to record the heating tape temperature

6.3 Flow System

In all three experiments, a vacuum was applied to the top of the soil column in order to simulate the process of soil vapor extraction. The vacuum pump used is pictured in Figure 6.10. The air pressure at the base of the soil column was vented to atmosphere, which leads to an upward flow of air through the soil column as shown in Figure 6.8. Flow meters are connected to the port at the bottom of the soil column (inlet) and between the top of the column and the vacuum pump (outlet). The vacuum pump exhaust is vented to a hood.

The flow meters used in this experiment were Riteflow® flow meters manufactured by Bel-Art, shown in Figure 6.9. Each flow tube used a single glass float. For air at 1 atm and a temperature of 70 °F, this flow meter can measure airflow from 28ml/min to 1249 ml/min. As gas enters through the opening at the bottom end, and exits through the opening at the top end, the upward pressure causes the float to rise. Flow takes place through the circular area between the float and the inside surface of the flow meter. As the float rises, the flow area increases due to the tapered bore of the flow meter. Dynamic equilibrium results when the upward force due to the air pressure balances the weight of the float. The height the float rise is related to a flow rate via a calibration chart supplied by Bel-Art. The flow tube for the inlet flow meter stopped working at the beginning of the third test so the inlet flow rate data is unavailable for that test.

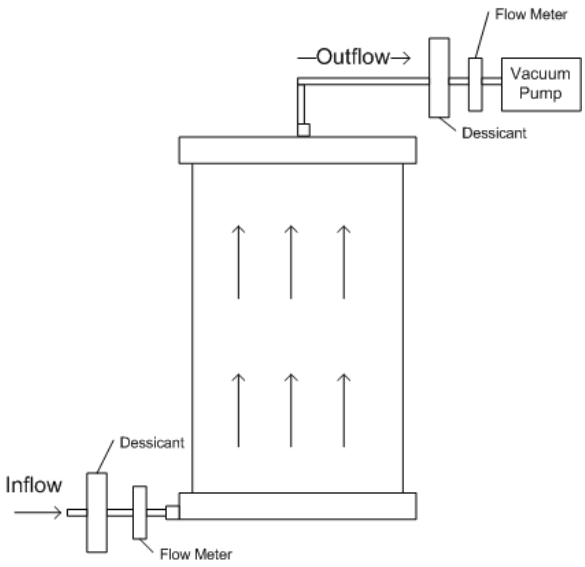

Figure 6.8: Flow system diagram

Figure 6.9: Riteflow flow meter: 65mm long with glass float

Figure 6.10: DryFast Collegiate Diaphragm Pump 2014 by Welsh

Laboratory gas drying units, shown in Figure 6.11, filled with indicating Drierite (desiccant) were placed inline between the effluent vapor sampling port and the flow meter to collect the moisture (diesel/water) that was removed from the column with the air flow. For the first test,

the drying unit was not used because significant moisture removal was not expected under room temperature conditions. For the second test one drying until was used. For the third test, two units were used in sequence due to the large quantity of water that was expected to be removed based on the observations from the second test. Unique to the third test, a drying unit was also placed at the air inlet port on the bottom cap. This was in an attempt to eliminate any water entering the column in the form of moisture in the laboratory air.

Figure 6.11: Drierite-filled laboratory gas drying unit

6.4 Vapor Sampling System

As mentioned, there are four vapor-sampling ports in the experiment. One effluent port installed immediately after the outlet in top end cap and three ports installed along the side of the cylinder. After the soil column has been compacted, a needle, showing in Figure 6.17, is inserted into the soil from the outside of the cylinder via an airtight fitting. The location of the tip of the needle is placed at the center of the soil column. The part of the needle that remains outside the cell is connected to a stopcock via a luerlock connection. The stopcock is closed when the port is not being used for sampling. Soil gas samples were extracted using 2.5 mL gas-tight syringes shown

in Figure 6.15, and then manually injected into a Gas Chromatographer to determine vapor-phase TPH concentration.

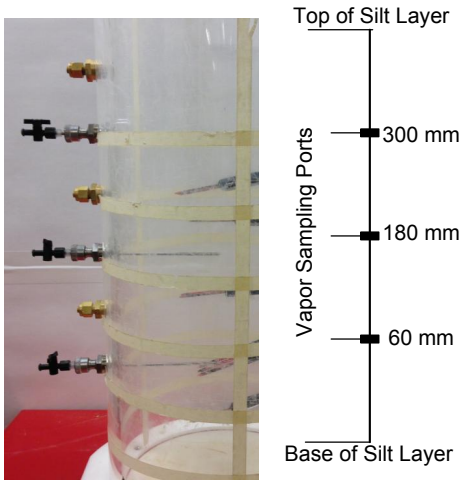

Figure 6.12: Profile vapor sampling port locations: depth from base (mm)

Figure 6.13: Effluent vapor sampling port

Figure 6.14: View of needle location as soil was being removed after the experiment was finished

Figure 6.15: SGE Analytical Science 2.5 mL gas-tight syringe with push-pull valve with Luer Lock termination

Figure 6.16: Push-pull valve with Luer Lock termination

Figure 6.17: 10 gauge, 127 mm long needle manufactured by Hamilton

Figure 6.18: Conical needle with side port to minimize soil blocking potential

6.5 Instrumentation

6.5.1 Dielectric and Temperature Sensors

The dielectric permittivity and temperature of the soil was measured using 5TM dielectric sensors manufactured by Decagon Devices of Pullman, WA. A picture of the sensor is shown in Figure 6.19. The sensors were placed at a uniform spacing of 60 mm at different depths along the centerline of the soil column, as shown in 6.22. The sensors measure temperature by an onboard thermistor that is mounted within the probe body. The sensors measure the dielectric constant of the soil using capacitance/frequency domain technology. The 5TM sensor measures the dielectric permittivity via a capacitor circuit created by its three prongs. The sensor generates a 70 MHz oscillating electromagnetic wave through its prongs. The prongs build up a charge, proportional to the dielectric of the soil. The sensor measures the charge time of the capacitor circuit and relates it to the dielectric permittivity of the soil. The sensor is connected to an ECH20 EM50 data logger manufactured by dielectric Devices and data is collected using the ECH20 Utility Software. The dielectric permittivity data was corrected to account for the impact of temperature on the sensor reading by subtracting an error of 0.01 per °C from the measured dielectric permittivity (Iezzoni and McCartney 2015).

Figure 6.19: Decagon 5TM dielectric sensors with embedded thermistor

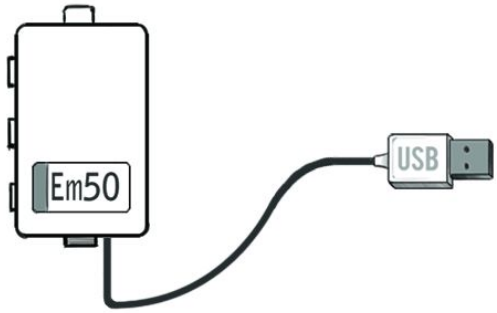

Figure 6.20: ECH20 EM50 data logger

Figure 6.21: View of dielectric sensor location as soil was being removed after the experiment was finished

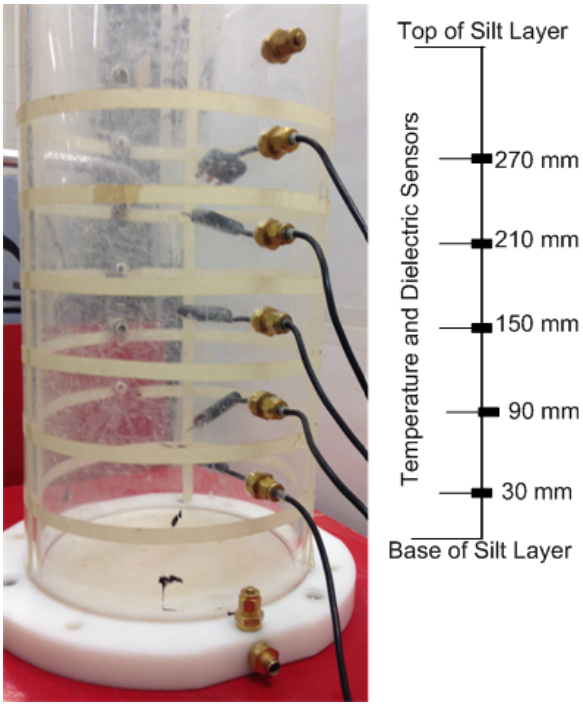

Figure 6.22: Dielectric sensor locations: From the base of the silt layer

6.5.2 USB Temperature and Relative Humidity Sensors

The EL-USB-2-LCD temperature and humidity USB data logger manufactured by Laskar was used to measure the temperature and relative humidity of the headspace inside the column. This is the area above the soil column but below the top cap. This sensor malfunctioned in the third experiment so no data is available for that test. Unique in the third test, another USB sensor was placed next to the cylinder to record fluctuations in the lab room temperature and relative humidity.

Figure 6.23: Temperature and humidity USB data logger

Chapter 7

Experimental Procedure

7.1 Soil Placement Procedures

7.1.1 Preparation of the Physical Model

The silt was moisture conditioned to the targeted gravimetric water content, before the soil was placed into the cylinder. The target gravimetric water content was 16% (corresponding to a water saturation of 45%) for test 1 and then was decreased to 13.5% (corresponding to a water saturation of 40%) for tests 2 and 3. An increase in temperature causes an increase in water vapor in both the soil pore space gas and the effluent gas. Samples with a high water vapor content can create problems with the Gas Chromatographer (GC). The moisture conditioning was done by spreading the soil out in a thin layer on a flat surface, spraying a fine mist of water onto the soil using a pressurized spray bottle, then mixing it by hand. This was repeated until the required mass of water was added to reach the target value. The moisture-conditioned soil was placed loosely in an airtight container and allowed to sit for 24 hours allowing the water content to homogenize. Samples were obtained to determine the average initial gravimetric water content using oven drying. Immediately before compaction, the soil was mixed with diesel fuel to achieve a concentration of 20,000 mg/kg of dry soil (corresponding to a diesel residual saturation of 7.1%). Using the gravimetric water content, diesel concentration and a target dry density of 1400 kg/m^3, the total density was calculated using Equation 7.1.

$$\rho_T = \frac{M_s + M_w + M_d}{V_T} \tag{7.1}$$

where M_s is the mass of the solids, M_w is the mass of the water, M_d is the mass of the diesel fuel, and V_T is the volume of the container.

7.1.2 Placement of the Sand Layer

Before the sand was placed in the container, the hole at the bottom was covered with filter paper to ensure that it did not get blocked with sand and impede airflow into the cylinder. The sand layer was placed in one lift by dry pluviation from a height of approximately 400 mm above the soil layer. After the sand was placed, the container was vibrated until the height of the sand layer reached a point that its dry density was 1739 kg/m^3. Then a ruler was used to level the surface of the sand. A thin layer of filter fabric was placed over the surface of the sand to prevent its mixing with the overlying silt layer.

7.1.3 Placement of the Silt Layer

The silt layer was placed and compacted into the container in six lifts. The projected heights of the six lifts were marked with tape wrapped around the outside of the container. Compaction was performed at every half lift to ensure uniformity of density. Kneading compaction using a constant pressure was used to compact the silt. After completing the compaction of each lift, the level of the soil surface was verified with a ruler to guarantee the correct height and a level surface. A dielectric sensor was placed at every half lift. A schedule of the lift levels used for compaction including the depths of the dielectric sensors and vapor-sampling ports for tests 2 and 3 is shown Table 7.1. For test 1, the height of the unsaturated silt layer height was only 300 mm. It followed the same compaction details for lifts one through five described in Table 7.1. The dielectric sensor locations were the same as in the other two tests but it only had one vapor sampling port placed in the soil column at 150 mm above the base.

After the silt layer was compacted, a USB sensor was placed on top of the soil layer and the top and bottom endplates were secured with four bolts running the length of the column and tightened down with nuts. An o-ring was fitted within a groove on either end of the column to

Table 7.1: Typical compaction details for the silt layer in tests 2 and 3

			Height (mm) above the base of the silt layer		
Lift Number	Thickness	Mass of soil (kg)	Layer	Dielectric sensors	Vapor sampling ports
1	60	3.99	60	30	60
2	60	3.99	120	90	
3	60	3.99	180	150	180
4	60	3.99	240	210	
5	60	3.99	300	270	300
6	60	3.99	360		

form a seal between the column and each endplate. Lastly, the needles for the vapor sampling ports were inserted into the soil from the outside of the cylinder via an airtight fitting so that the tip of each needle was at the center of the soil column. before inserting the needles, a small length of all-thread of the same diameter as the needle was used to create an opening in the soil. This permitted insertion of the needle into the center of the compacted soil layer with minimal disturbance.

7.2 Testing Procedure

7.2.1 Heating Phase

Three tests were performed at three different target soil temperatures: 23 °C (room temperature), 40 °C and 60 °C. For all three tests, the temperature of the soil was initially at room temperature of approximately 22 to 23 °C. For the first test no heating was required. For the second and third test the heating tape was used to heat the soil to the target soil temperature. First, the variable voltage meter, connected to the heating tape, was set to 50% while the soil was being increased from room temperature to the targeted testing temperature. Then the voltage meter was decreased to 10% for the rest of the experiment. To maintain the targeted soil temperature (+/- 5 °C) throughout the rest of the experiment, the automatic timer was set to turn the heating tape on and off in predetermined cycles, with a shorter cycle leading to higher temperatures. Al-

though this leads to periodic fluctuations in temperature at the boundary of the specimen, the soil temperature within the column reaches a relatively stable value. Also, the length and frequency of these intervals changed as the experiment progressed because the soil was drying out and thus required less energy to keep at the targeted temperature. This led to slight changes in the average soil temperature throughout the test.

7.2.2 Vapor Extraction Phase

After the soil was heated to the targeted temperature, the vacuum was turned on. Using the vacuum regulator, the vacuum was increased until the target flow rate of 500mL/min was achieved. A flow rate of 500 ml/min corresponds to a pore volume exchange rate of approximately 103 pore volumes per day. Calculations for the pore volume exchange rate are shown in Equations 7.2 and 7.3.

$$\begin{aligned}\text{Time to exchange one pore volume} &= \frac{\text{Volume of voids in soil } (\text{m}^3)}{\text{Flow rate } (\text{m}^3/\text{day})} \\ &= \frac{6.98 \times 10^{-3}}{0.72} = 9.70 \times 10^{-3} \text{ days}\end{aligned} \tag{7.2}$$

$$\text{Pore volume exchange rate} = 1/(9.70 \times 10^{-3}) = 103.14 \text{ (pore volume/day)} \tag{7.3}$$

A typical pore volume exchange rate in the field is 1 to 10 pore volumes per day. Laboratory experiments are frequently run at higher than typical field pore volume exchange rates. For example, the pore volume exchange rates in the experiments performed by Park et al. (2005) ranged from 379 to 3030 pore volumes per day. Poppendieck et al. (1999a) used a pore volume exchange rate of around 800 pore volumes per day in their experiments. It is acceptable to use higher rates in laboratory situations, but it is important to understand the implications of the higher rates on remediation times. SVE performed in the field at sites with typical contaminant residual saturation levels can take multiple years to complete, while laboratory experiments usually have a duration of a few days to a few weeks depending on the size of the soil column.

After the desired flow rate was achieved, the vacuum was then left on until the experiment was over. The vacuum gauge reading and inflow and effluent flow rates were recorded every few hours in the beginning of the experiment and at longer intervals as the experiment progressed. The total running vacuum time for each experiment is given in Table 7.2. The total running vacuum time is different for each experiment. For tests 2 and 3 the experiment was run until the vapor-phase total petroleum hydrocarbon (TPH) concentration in the effluent reached a steady state. Test 1 was stopped before steady state was reached. Technical difficulties at the start of the test delayed the experiment and access to the GC ended before the vapor-phase TPH concentration in the effluent could reach steady state.

Table 7.2: Total vacuum running time for each experiment

Test	Total vacuum running time (hrs)
1	97.0
2	130.5
3	150.3

7.2.2.1 Water Removal Collection System

In the two heated tests, laboratory gas drying units filled with color-indicating Drierite were placed inline between the effluent sampling port and the flow meter. For test 2, only one drying unit was needed. For test 3, two units were needed due to the higher amount of water removed from the soil. When the Drierite changed color, indicating that it was exhausted, the cylinder was disconnected, weighed, emptied, filled with new Drierite, weighed again and then reconnected. The mass of water that was removed between each replacement of the drying unit was calculated by subtracting the mass of the dry Drierite from the wet Drierite.

7.2.2.2 Vapor Sampling Schedule and Procedure

Vapor samples were obtained at different time intervals throughout the soil vapor extraction phase. For the first 24 hours vapor samples were taken every 4-6 hours. After that, vapor samples

were only taken every 8-12 hours. Vapor samples were taken from the three sampling ports along the height of the soil column and the one outflow sampling port.

Heated (only for the experiments involving elevated temperatures) gas tight syringes with valves were attached to the stopcock via luer lock connections. The syringe (with the valve set to the open position) is connected to the stopcock. The stopcock is then opened. To flush the needle, 2 mL of pore gas is drawn from the port then discarded. Then a sample is taken. The volume of the same was 2.5 mL in test 1 and 1 mL in tests 2 and 3. The syringe valve and stopcock are both set to the closed position and the syringe is detached from the stopcock. The syringe containing the vapor sample was then placed on a temperature-regulated heating plate and maintained at the same temperature as the soil until it could be injected into the GC for testing.

Chapter 8

Experimental Results

8.1 Overview

The results from the three tests are presented in graphical form in this section. The timescale for all the graphs shown in this section start from when the silt was compacted to multiple hours after the vacuum was discontinued. The graphs are accompanied with vertical dotted lines that correspond with the ON/OFF vacuum interval.

8.2 Test 1: Average Soil Temperature of 23 °C

Test 1 was conducted at room temperature. It was the first test performed and although some data was collected there were multiple errors and malfunctions that occurred. Because of this, only a portion of the data presented for the other two tests can be reported. Specifically the temperature and dielectric permittivity data is unavailable. Also, there is no data on the cumulative mass of water removed for this test because significant water removal was not expected at room temperature. After the experiment was conducted the final water saturation data shows that some water did end up being removed, likely due to evaporation associated with the lower vapor pressure induced by the vacuum boundary condition.

The initial saturations of water, air and diesel for the test at 23 °C are given in Table 8.1 and shown graphically in Figure 8.2. This figure shows that the water saturation and diesel content are assumed to be constant with height at the beginning of the test. The air saturation of 48% is high enough that the air phase is likely initially continuous across the soil layer.

Table 8.1: Saturations and Initial Diesel Concentration

Saturations	
Water	0.45
Air	0.48
Diesel	0.07
Initial diesel concentration in dry soil	20,000 mg/kg

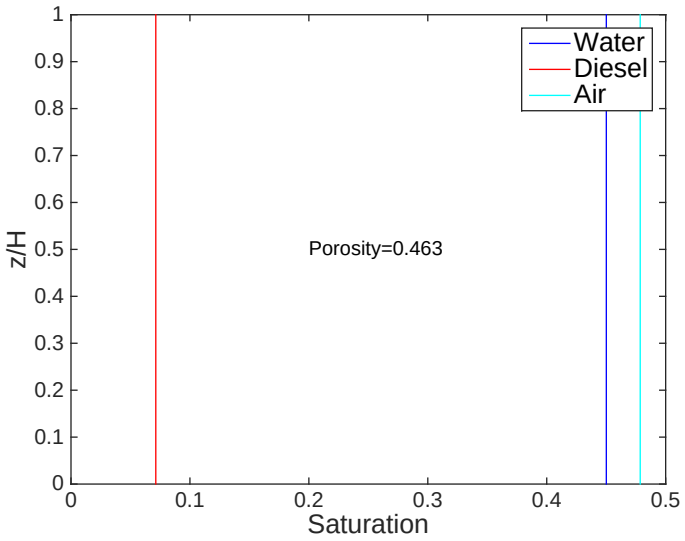

Figure 8.1: 23 °C test: Initial water, diesel and air saturations

The vacuum schedule for the test at 23 °C is presented in Table 8.2. The total vacuum duration in this test was 97 hours. The vacuum pump had to be turned off for a few hours after the start of the test due to technical difficulties. These gaps in vacuum suction are given in Table 8.2. These technical difficulties at the start of the test also delayed the experiment, forcing the experiment to be terminated early and explains why the total vacuum time for this test is much less for the other two tests. The vacuum suction in kPa applied to the sample is plotted with time in Figure 8.2. The dotted lines in the figures that follow correspond with the ON/OFF vacuum interval

Table 8.2: Test 1: Vacuum schedule

Event	Elapsed Time (hrs)
Vacuum ON	1.73-8.50
Vacuum duration	6.77
Vacuum OFF(technical difficulties)	8.50-29.50
Vacuum OFF duration	21
Vacuum ON	29.50-119.73
Vacuum duration	90.23
Total vacuum duration	97

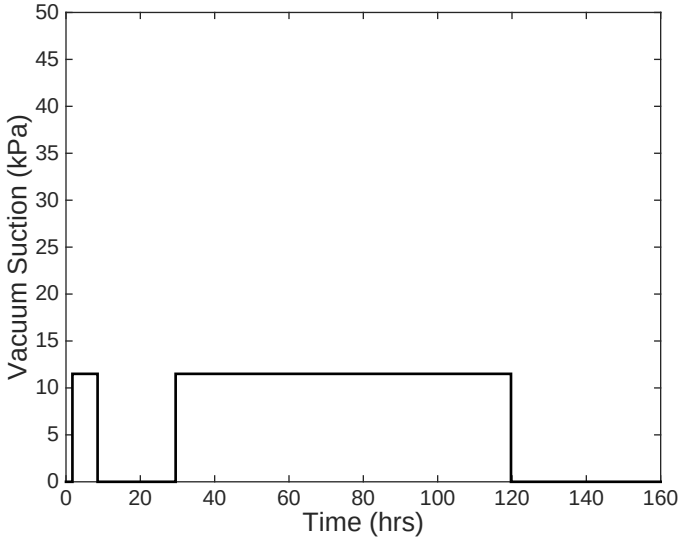

Figure 8.2: 23 °C test: Vacuum on/off with time.

Figures 8.3 and 8.4 show the temperature and relative humidity, respectively, recorded in the test at 23 °C by the sensor placed on top of the silt layer inside the column. Since no external heat was applied to this section the temperature remains relatively constant around 22-23 °C. The slightly higher portion at the beginning of the test before the vacuum was applied is likely due to the fact that the soil column after assembled, was moved to a different location in the building that had access to a hood.

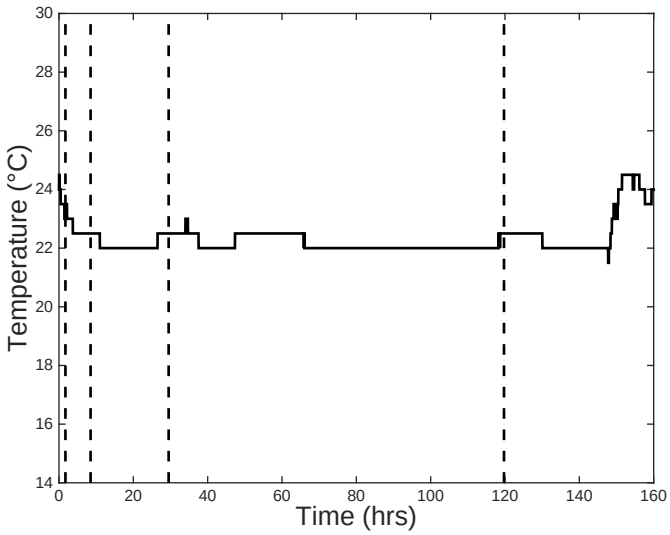

Figure 8.3: 23 °C test: Temperature of the air above the silt in the cylinder

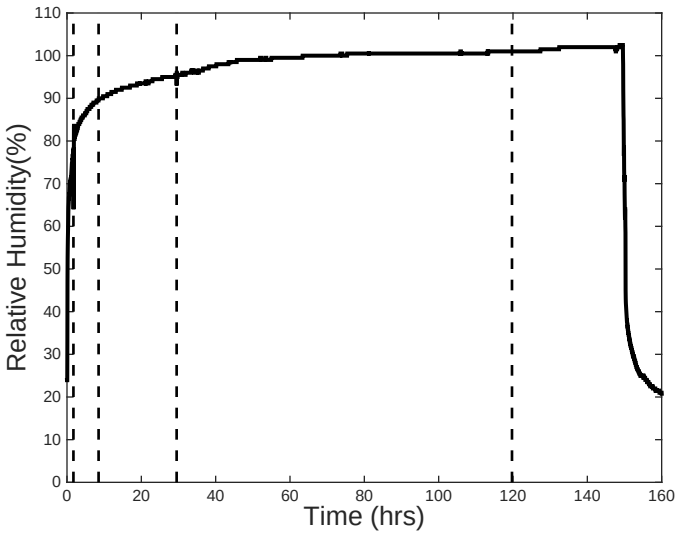

Figure 8.4: 23 °C test: Relative humidity of the air above the silt in the cylinder

The water saturation at the start and end of the experiment is presented in Figure 8.5. Due to the technical difficulties mentioned above, the test had to be stopped early, and the final water saturation and estimated total water storage change of 0.208 kg was taken after only 97 hours of applied vacuum. It is very possible that if the experiment were allowed to continue the soil would

continue to dry out and achieve uniform water saturation along the height of the soil column.

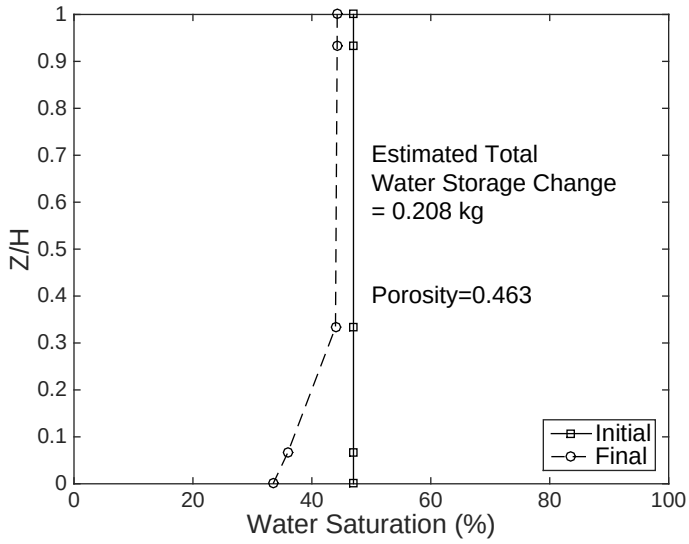

Figure 8.5: 23 °C test: Initial and final water saturation profiles

The airflow entering and leaving the sample for the test at 23 °C is given in Figure 8.6. The flow rate for the first 6.75 hours is unknown because the correct float type needed for the desired flow range was not installed in the flow tube during this interval.

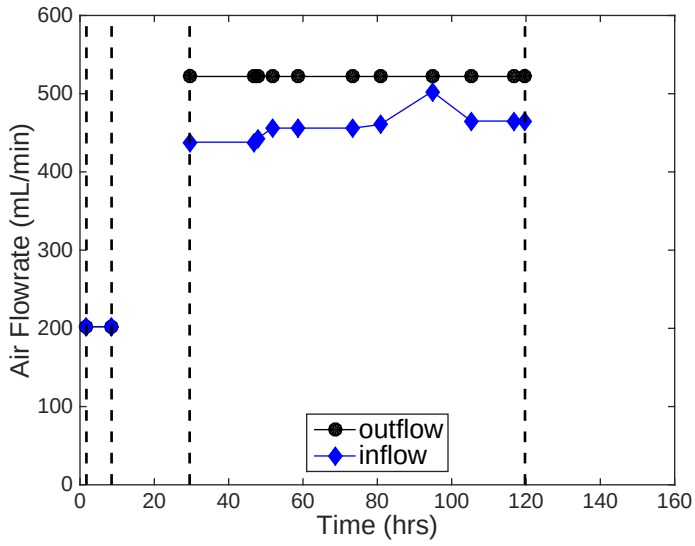

Figure 8.6: Inflow and outflow represents the airflow entering the bottom of the column and the airflow exiting the top of the column, respectively.

The vapor-phase TPH concentration of the effluent is given in Figure 8.7 followed by the TPH concentration of the soil gas in the pore space 150mm above the base of the column in Figure 8.8. The GC data for the first part of this test is unavailable due to the technical difficulties mentioned above.

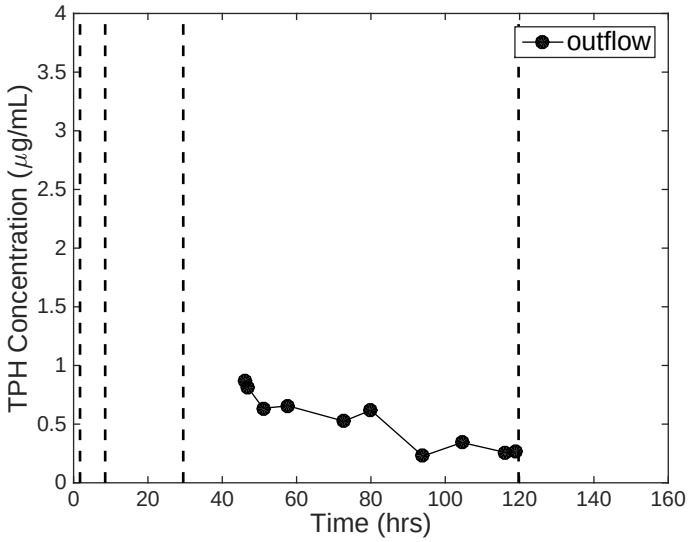

Figure 8.7: 23 °C test: The vapor-phase TPH concentration of the effluent

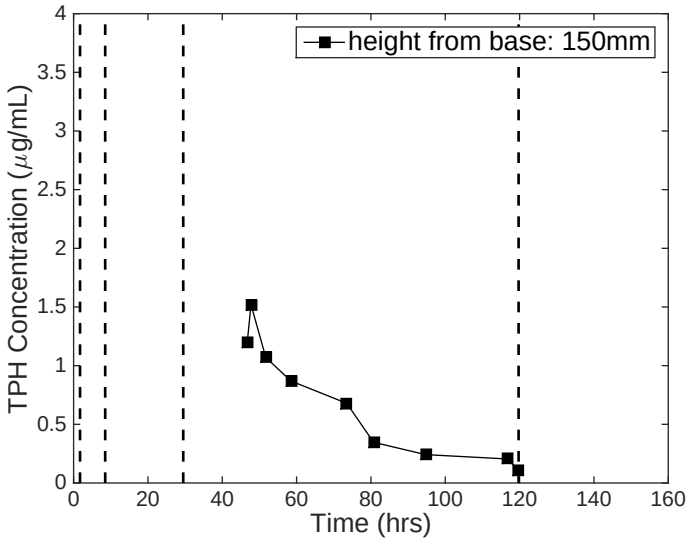

Figure 8.8: 23 °C test: The TPH concentration of the soil gas in the pore spaces 150mm above the base of the column.

8.3 Test 2: Average Soil Temperature of 40 °C

Test 2 was conducted at an average soil temperature of 40 °C. It was the second test performed and the first of the thermal tests. The heating tape was wrapped around the outside of the cylinder containing the soil. The initial saturations of water, air and diesel are given in Table 8.3 and shown graphically in Figure 8.9. This figure shows that the water saturation and diesel content are assumed to be constant with height at the beginning of the test. The air saturation of 53% is high enough that the air phase is likely initially continuous across the silt layer.

Table 8.3: Saturations and Initial Diesel Concentration

Saturations	
Water	0.40
Air	0.53
Diesel	0.07
Initial diesel concentration in dry soil	20,000 mg/kg

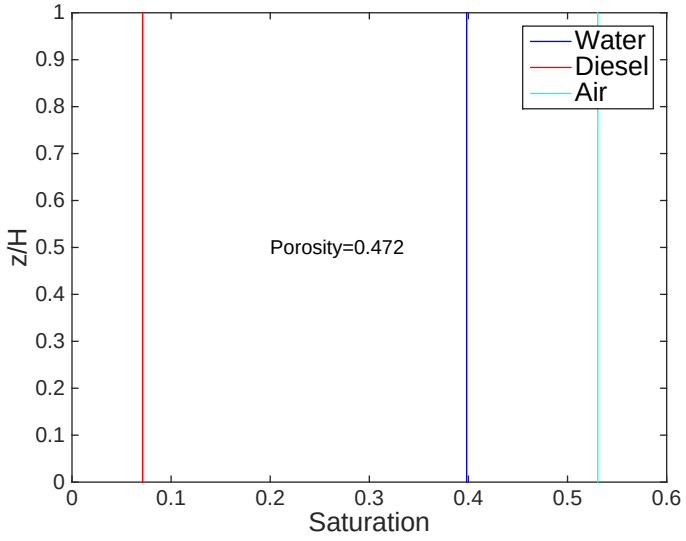

Figure 8.9: 40 °C test: Initial water, diesel and air saturations

The vacuum schedule for the test at 40 °C is presented in Table 8.4. The total vacuum

duration in this test was 130.5 hours. The discrepancy between the end of the heating and the end of the vacuum is due to human error. The heating tape was not properly connected to the automatic timer after the last timer program adjustment. The vacuum suction in kPa applied to the sample is plotted with time in Figure 8.10. The black dotted lines in the figures that follow correspond with the ON/OFF vacuum interval. The red dotted line corresponds to the time the heating tape was shut off.

Table 8.4: 40 °C test: Heating and vacuum schedule

Event	Elapsed Time (hrs)
Heating up column	0-5.58
Vacuum On	5.58-136.08
Heat Ended	@121.08
Vacuum duration	130.5

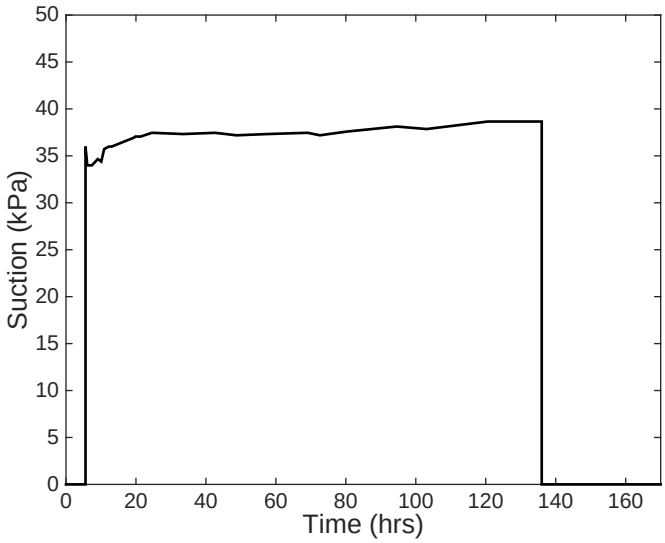

Figure 8.10: 40 °C test: Vacuum on/off with time.

Figures 8.11 and 8.12 shows the temperature and relative humidity, respectively, recorded in the test at 40 °C by the sensor placed on top of the silt layer inside the column.

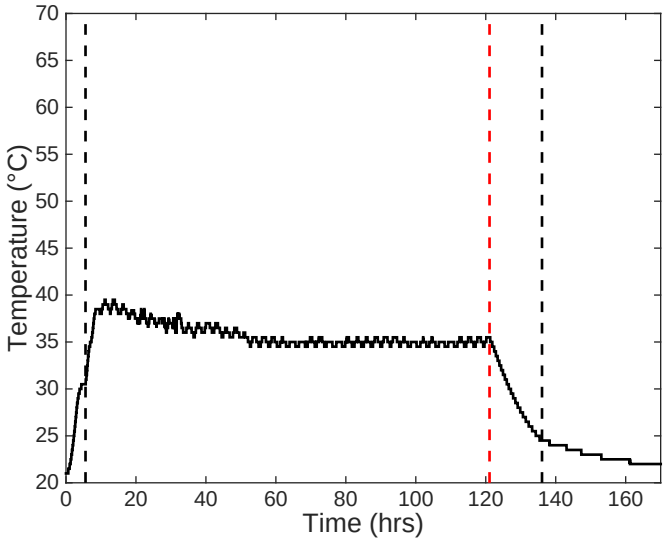

Figure 8.11: 40 °C test: Temperature of the air above the silt in the cylinder

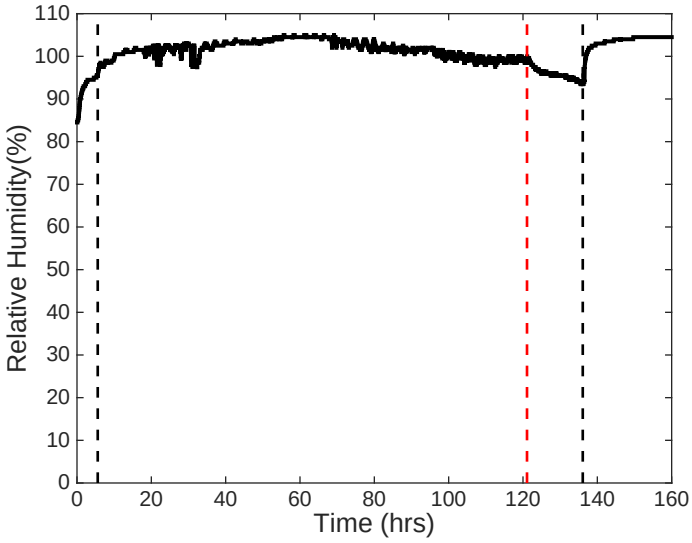

Figure 8.12: 40 °C test: Relative humidity of the air above the silt in the cylinder

The heating tape temperature and the silt temperature in the center of the column (150 mm above the base) for the test at 40 °C is shown in Figure 8.13. Figure 8.14 shows the temperature of the silt at different locations of the column for the same test.

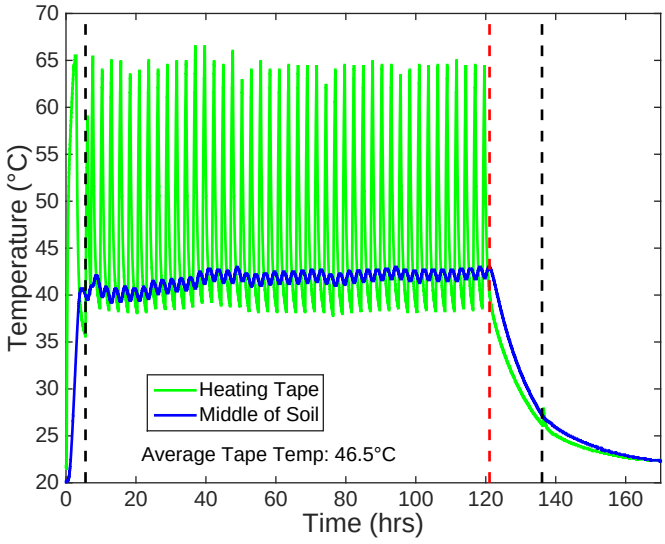

Figure 8.13: 40 °C test: Heating tape temperature plotted with the silt temperature in the center of the column (150 mm above the base)

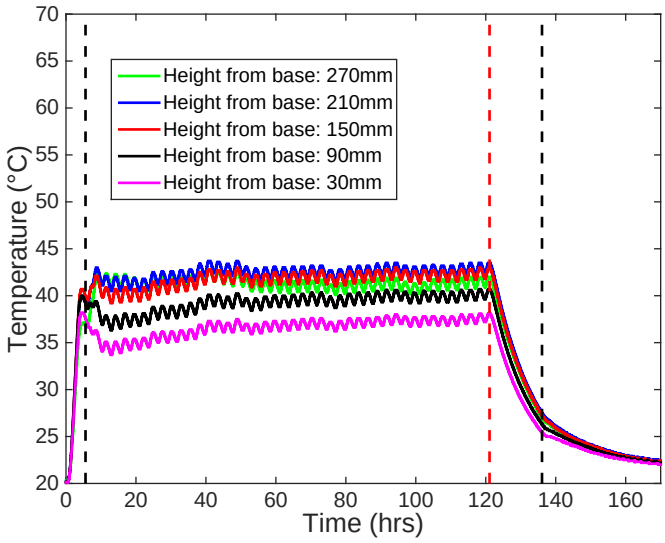

Figure 8.14: 40 °C test: Soil temperature at different locations in the column

The change in dielectric permittivity for the test at 40 °C is shown in Figure 8.15. The cumulative mass of water removed from the test at 40 °C is given in Figure 8.16 and the water saturations at the start and end of the experiment are presented in Figure 8.17.

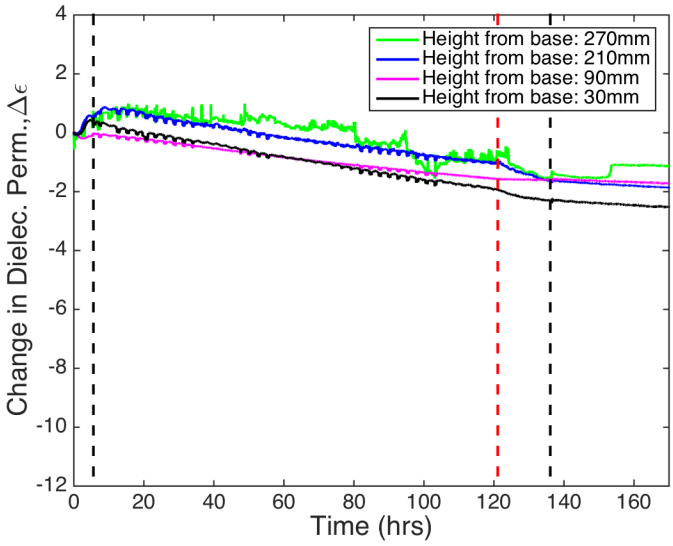

Figure 8.15: 40 °C test: The change in dielectric permittivity at different locations in the column

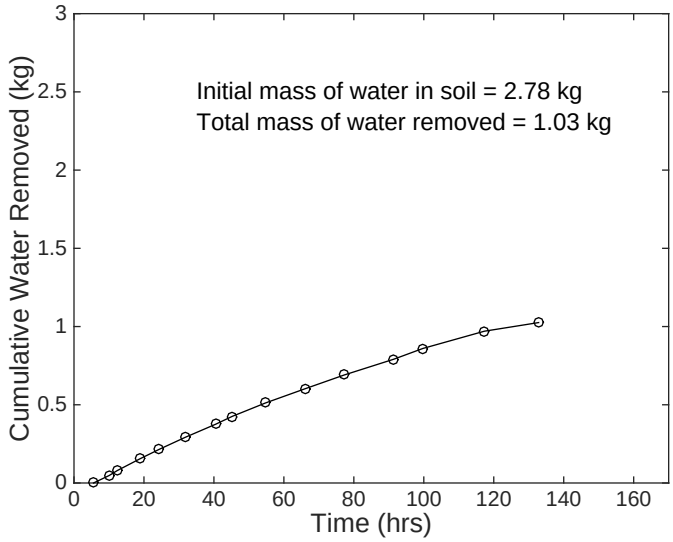

Figure 8.16: 40 °C test: Cumulative mass of water removed

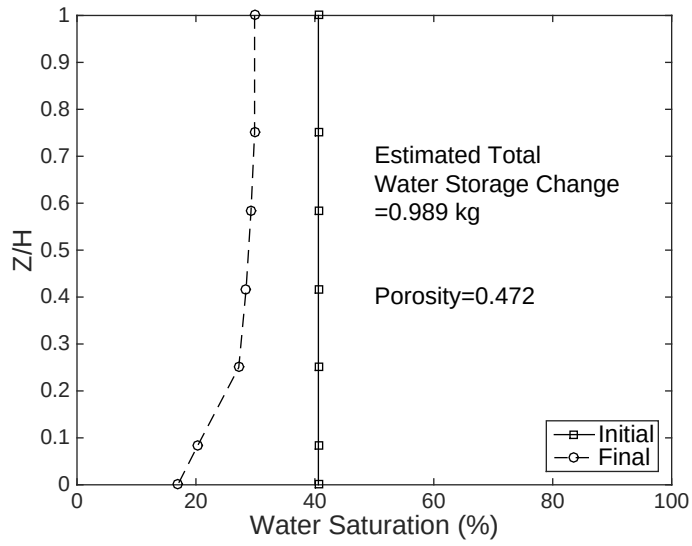

Figure 8.17: 40 °C test: Initial and final water saturation profiles

The airflow entering and leaving the sample for the test at 40 °C is given in Figure 8.18. The flow rate was not intentionally varied but believed to be the result of water and diesel collecting in the outflow lines and instrumentation and inhibiting flow.

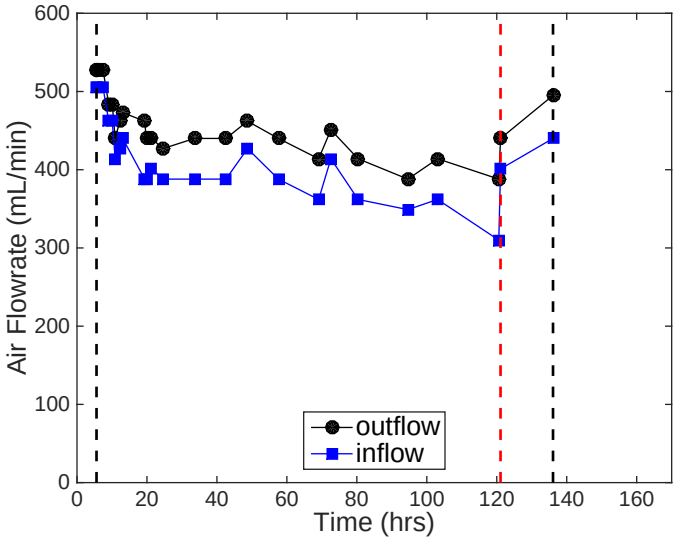

Figure 8.18: 40 °C test: Airflow rates. Inflow and outflow represents the airflow entering the bottom of the column and the airflow exiting the top of the column, respectively.

The TPH concentration values of the effluent is given in Figure 8.19 followed by the TPH concentration of the soil gas in the pore space at different locations in the column in Figure 8.20. The data from the location that is 60 mm is not shown here because the port malfunctioned during testing.

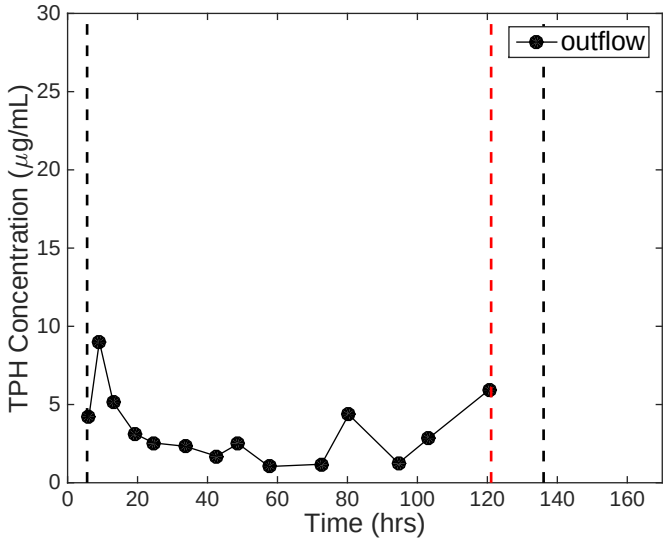

Figure 8.19: 40 °C test: The TPH concentration of the effluent

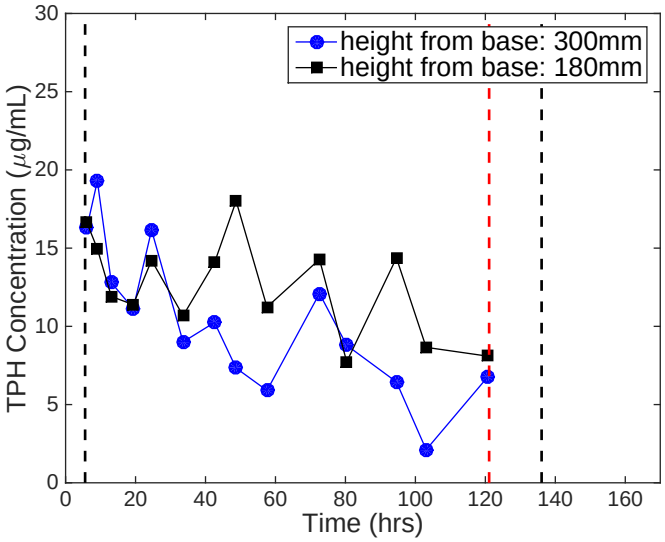

Figure 8.20: 40 °C test: The TPH concentration of the soil gas in the pore spaces at two different heights above the base of the column

8.4 Test 3: Average Soil Temperature of 60 °C

Test 3 was conducted at an average soil temperature of 60 °C. It was the third test performed and the last of the thermal tests. The initial saturations of water, air and diesel are given in Table 8.5 and shown graphically in Figure 8.21. This figure shows that the water saturation and diesel content are assumed to be constant with height at the beginning of the test. The air saturation of 53% is high enough that the air phase is likely initially continuous across the silt layer.

Table 8.5: Saturations and Initial Diesel Concentration

Saturations	
Water	0.40
Air	0.53
Diesel	0.071
Initial diesel concentration in dry soil	20,000 mg/kg

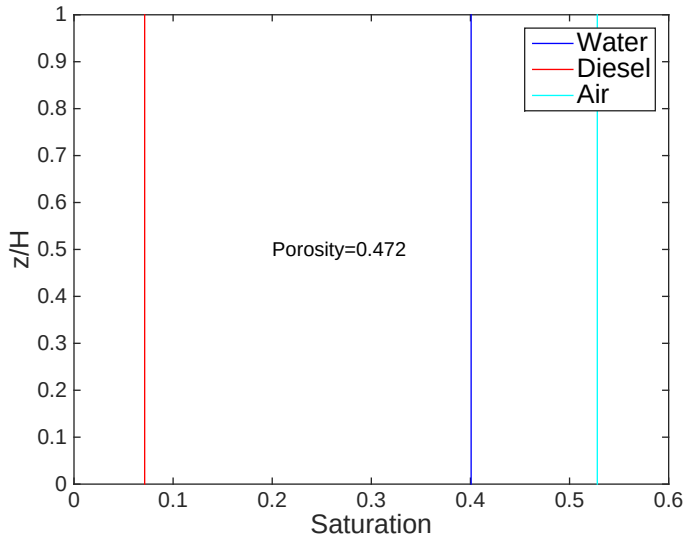

Figure 8.21: 60 °C test: Initial water, diesel and air saturations

The vacuum schedule for the test at 60 °C is presented in Table 8.6. The total vacuum duration in this test was 150.34 hours. The vacuum suction in kPa applied to the sample is plotted

with time in Figure 8.22. The dotted lines in the figures that follow correspond with the ON/OFF vacuum interval

Table 8.6: Test 3: Heating and vacuum schedule

Event	Elapsed Time (hrs)
Heating up column	0-15.66
Vacuum On	15.66-166
Heat Ended	@ 166
Vacuum duration	150.34

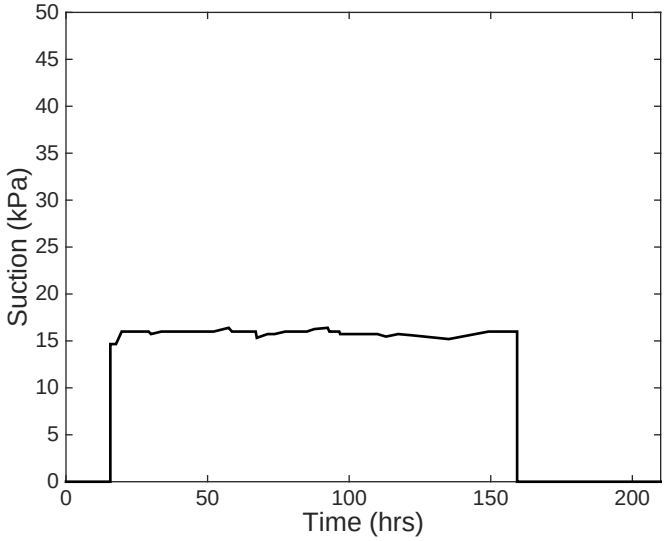

Figure 8.22: 60 °C test: Vacuum on/off with time.

Unique to this test is that the temperature and relative humidity for the laboratory were monitored during the experiments, as shown in Figure 8.23. This data is unavailable in the first two tests, as the temperature and relative humidity of the lab was initially assumed to be constant. In the third test, a sensor was set out in the lab, next to the cylinder to see how accurate that assumption was. This data should be accompanied with the temperature and relative humidity of the headspace above the silt but unfortunately that sensor malfunctioned in this test so no data is available.

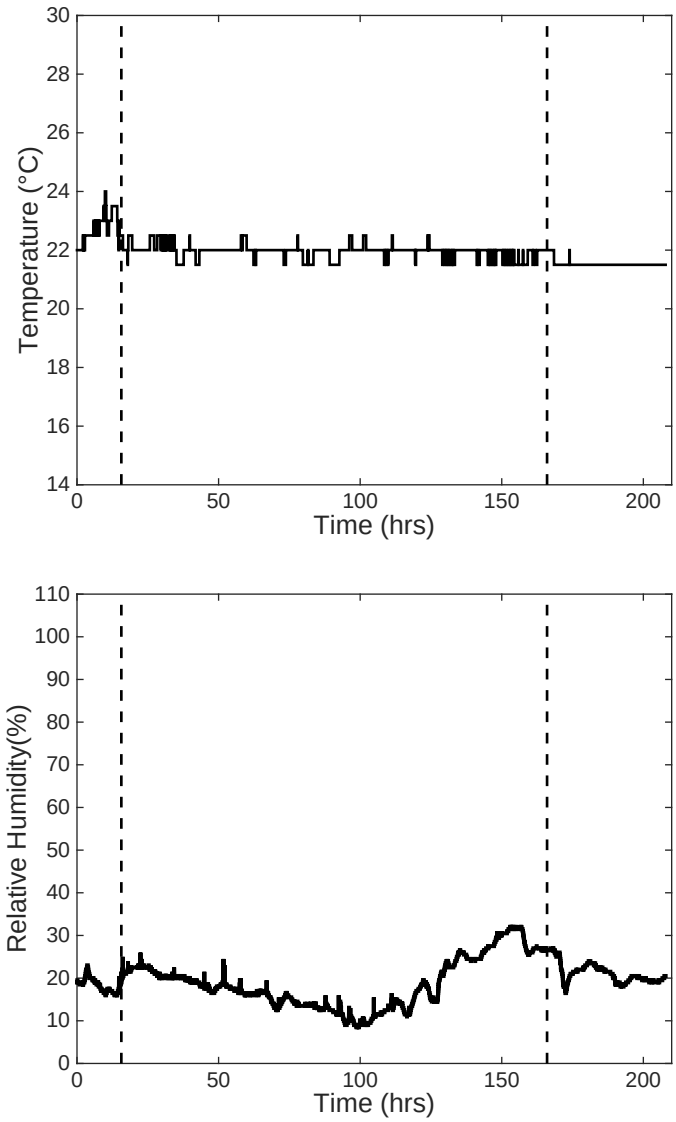

Figure 8.23: 60 °C test: Temperature and relative humidity of the room the column was in

The heating tape temperature and the silt temperature in the center of the column (150 mm above the base) for the test at 60 °C is shown in Figure 8.24. Figure 8.25 shows the temperature of the silt at different locations of the column for the same test.

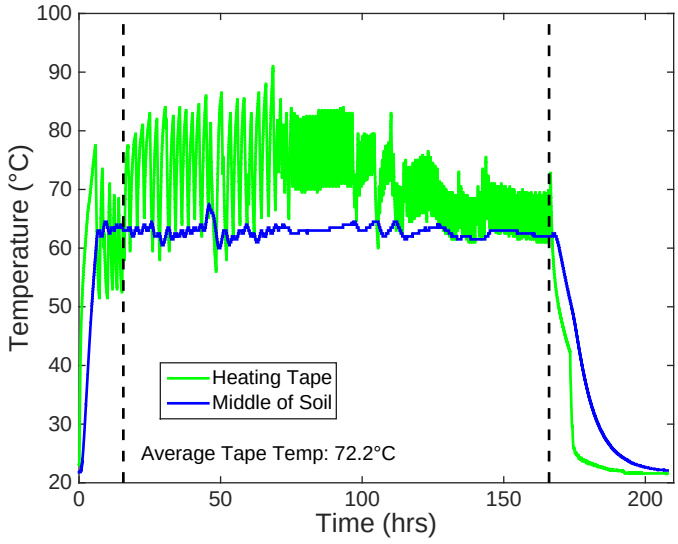

Figure 8.24: 60 °C test: Heating tape temperature plotted with the silt temperature in the center of the column (150 mm above the base)

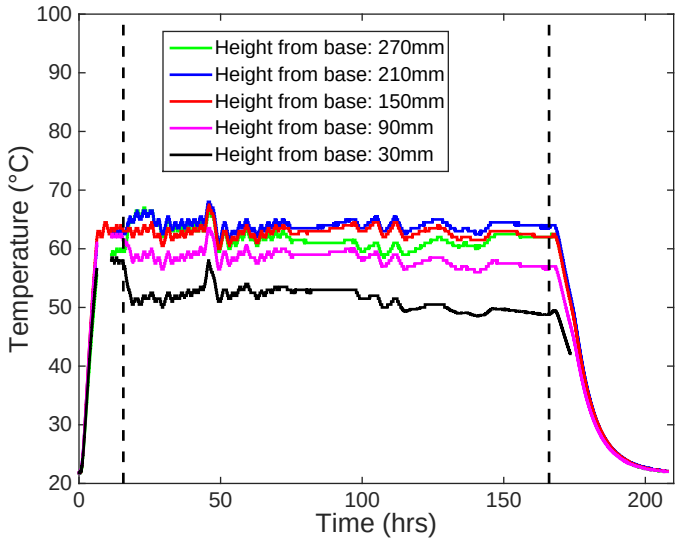

Figure 8.25: 60 °C test: Soil temperature at different locations in the column

The change in dielectric permittivity for the test at 60 °C is shown in Figure 8.26. The cumulative mass of water removed from the same test is given in Figure 8.27 and the water saturations at the start and end of the experiment are presented in Figure 8.28.

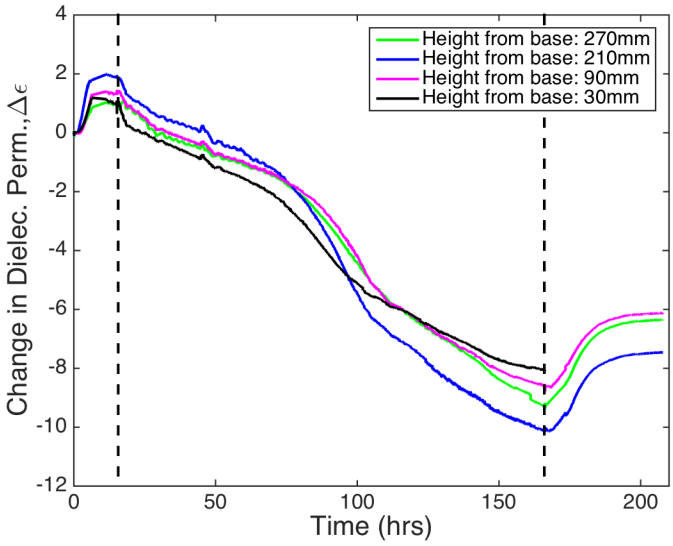

Figure 8.26: 60 °C test: The change in dielectric permittivity at different locations in the column

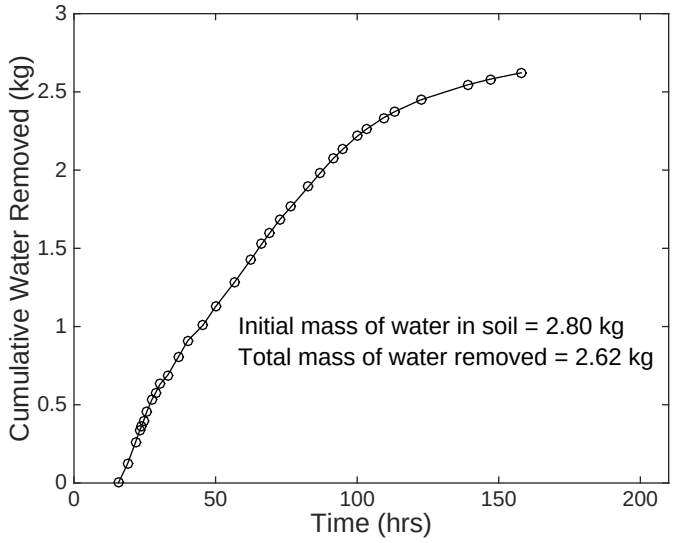

Figure 8.27: 60 °C test: Cumulative mass of water removed

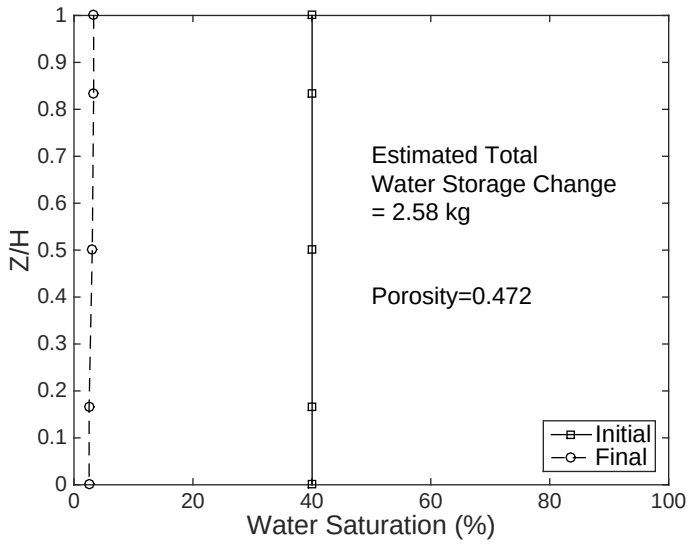

Figure 8.28: 60 °C test: Initial and final water saturation profiles

Another unique set of data for the test at 60 °C is presented in Figure 8.29. This data represents the TPH concentration of the soil gas in the pore spaces at three different heights above the base of the column before any vacuum was applied. The first three samples were taken before any heat was applied to the silt (denoted by the circle data points). The square data points represent samples taken after the silt reached an average temperature of 60 °C but before any vacuum was applied.

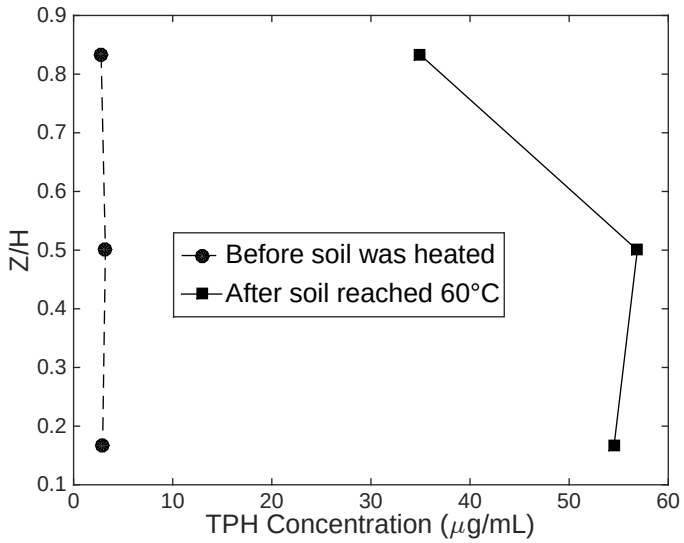

Figure 8.29: 60 °C test: The TPH concentration of the soil gas in the pore spaces at three different heights above the base of the column before the vacuum was applied

The airflow entering and leaving the sample for the test at 60 °C is given in Figure 8.30. The flow rate was not intentionally varied but believed to be the result of water and diesel collecting in the outflow lines and instrumentation and inhibiting flow.

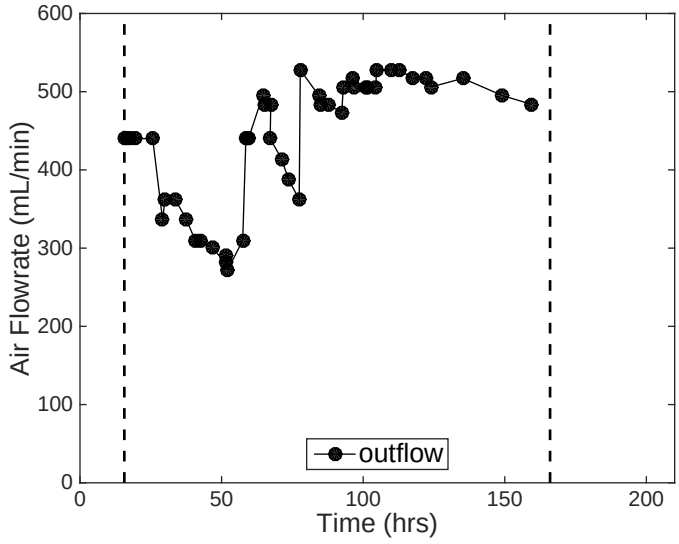

Figure 8.30: 60 °C test: Airflow rates. Outflow represents the airflow exiting the top of the column. There is no inflow data for this test because of a flow meter malfunction

The vapor-phase TPH concentration of the effluent is given in Figure 8.31 followed by the TPH concentration of the soil gas in the pore space at different locations in the soil column in Figure 8.32.

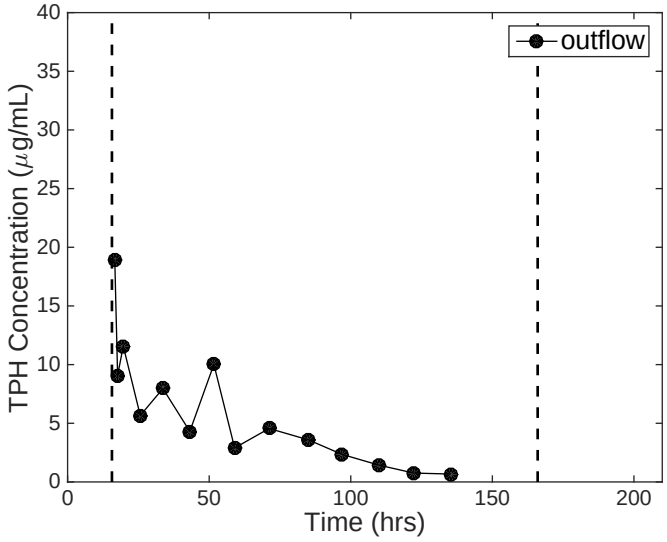

Figure 8.31: 60 °C test: The vapor-phase TPH concentration of the effluent

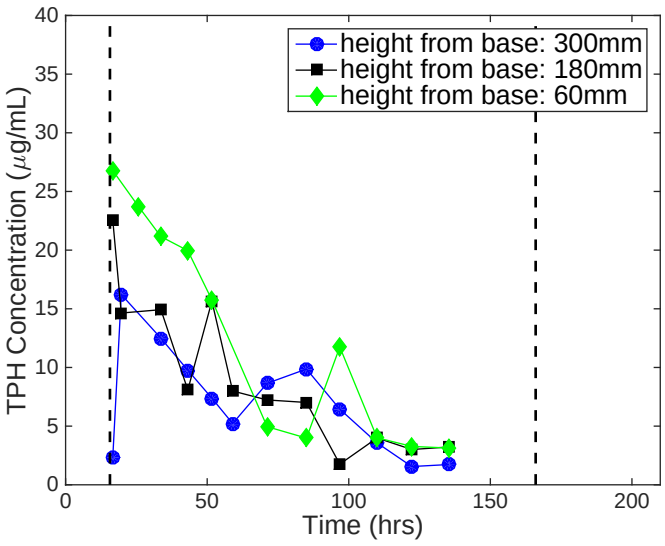

Figure 8.32: 60 °C test: The TPH concentration of the soil gas in the pore spaces at three different heights above the base of the column

Chapter 9

Analysis

In an attempt to correctly compare the three tests, the results presented below are given in terms of total running vacuum time where zero corresponds to the start of the vacuum. Any breaks in application of the vacuum are ignored. The airflow rates at the effluent side of the soil column are shown in Figure 9.1. Although a large amount of variability is observed in the data, the goal of the vacuum application was to maintain a constant airflow rate between 400 and 500 mL/min. It was easier to obtain a constant flow rate after a greater amount of water had been removed from the soil, which is why the airflow rate stabilizes over time in the two heated tests. The flow meters used in this study were very sensitive to water vapor condensing inside the flow tubes and were prone to inaccurate flow readings. The gas drying unit full of desiccant was placed inline in an attempt to dry the air before it entered the flow meter. however, during the beginning of the heated tests, when the water removal rate was the highest, it was difficult to change the drying units as often as was required. The decrease in flow rate for the test at 60 °C should be taken into consideration when analyzing the concentration in the effluent and the mass removal of the contaminant. Assuming that the flow meters were accurate and the test at 60 °C did actually see a decrease to 300 ml/min,10 hours into the experiment, which lasted for 30 hours, then the water removed and the concentrations in the effluent and total mass removed will be slightly less than what would be predicted for an average flow rate of 500 ml/min.

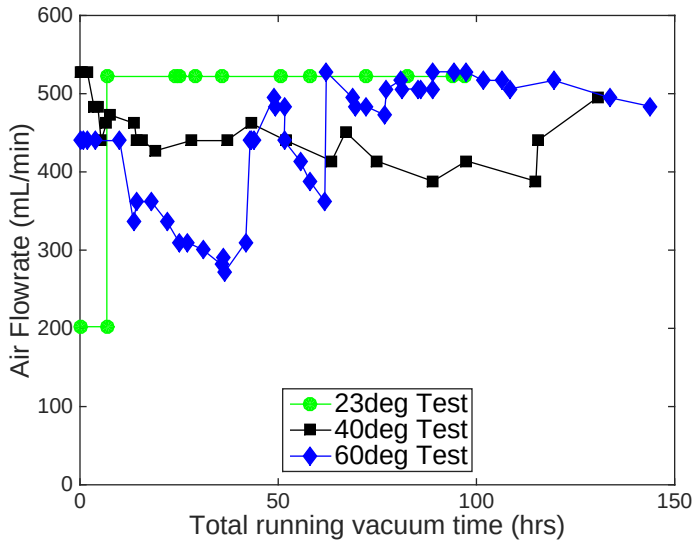

Figure 9.1: Effluent flow rate

A summary of the cumulative amount of water removed during the tests at 40 and 60 °C is shown in Figure 9.2. It is clear that a much larger amount of water was withdrawn from the column with the higher temperature. The mass of water removed after 90 hrs and 115.5 hours is estimated for all three tests and given in Table 9.1. After 115.5 hours, the removal in the test at 60 °C was 2.55 times that removed in the test at 40 °C. This is most likely related to the increase in saturated vapor pressure with temperature. As observed in Figure 8.12, the relative humidity data for the test at 40 °C reaches 100% very quickly and maintains that value until the heat is turned off. This implies that the vapor pressure of water in the air leaving the column is fully saturated with water. Since the saturated vapor pressure of water at 60 °C is 2.70 times the saturated vapor pressure at 40 °C, as shown in Table 9.2, the amount of water removed in each test is reasonable.

Table 9.1: Mass of water removed after 90 and 115.5 hours of applied vacuum

Test	Initial mass of water (kg) in soil	Mass of water (kg) removed		Percent removed	
		After 90 hrs	After 115.5 hrs	After 90 hrs	After 115.5 hrs
23 °C	2.62	0.21	NA	8.02 %	NA
40 °C	2.78	0.86	0.98	30.94 %	35.25 %
60 °C	2.80	2.47	2.50	88.21 %	89.29 %

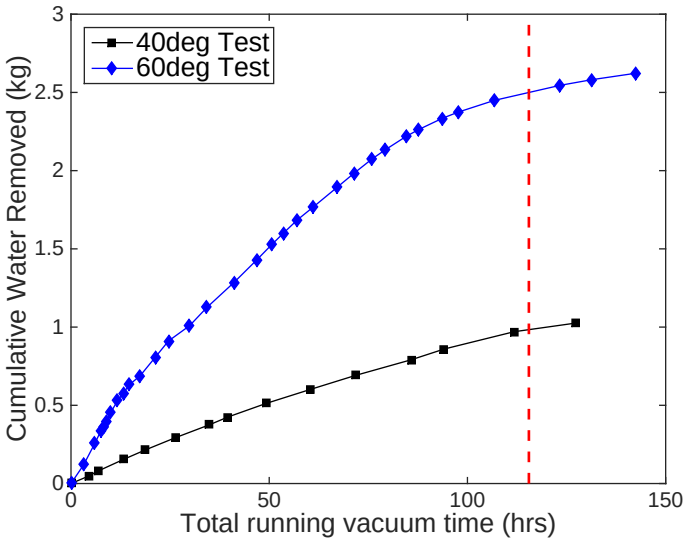

Figure 9.2: Cumulative mass of water removed

Table 9.2: Saturated vapor pressure of water at different temperatures

	Vapor Pressure (kPa)		
	20 °C	40 °C	60 °C
Water	2.81	7.37	19.92

During the heating process, the dielectric permittivity of the soil, as presented in Figure 8.15 and Figure 8.26, showed an initial increase at the beginning, which corresponds with the upward flow of water and LNAPL past the location of each of the sensors. An interesting observation is that the dielectric permittivity at all of the locations decreased at the same rate. This is possibly because the soil was initially relatively dry and the air permeability is uniform across the soil layer, leading to uniform drying. Some variability in the response of the sensors at different depths was observed, potentially due to the impact of preferential airflow paths through the soil layer.

Figure 9.3 shows the vapor-phase total petroleum hydrocarbon (TPH) concentrations for the effluent in all three tests. They follow the same pattern as the results presented by Park et al. (2005) and are characterized by an initial sharp increase in effluent concentration followed by a sharp drop off. The peak for the test at 60 °C is the highest, followed by the test at 40 °C. Although the data for the beginning of the test at 23 °C is missing, assuming trends in literature, the beginning vapor-phase TPH concentrations for the test at 23 °C are likely lower than in the other two tests.

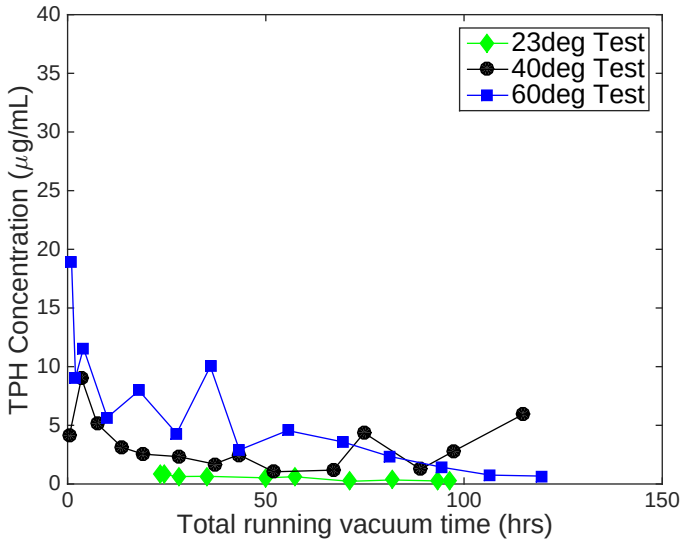

Figure 9.3: A comparison of the TPH concentration of the effluent in each test

Figures 9.4 and 9.5 show comparisons of the TPH concentrations of the soil gas in the pore space at 150-180 m and 300 m above the base of the column. As mentioned before, the data

from the soil gas in the pore spaces at 60 m above the base of the column for the test at 40 °C is unavailable so a comparison is not shown. As expected, the TPH concentration decreases with time in all three locations. Also as expected, the TPH concentrations for the higher temperature tests are greater than the tests at the lower temperatures. It is also interesting to remark on the trend seen when the TPH concentrations for the soil gas in the pore spaces for each location are compared within each test as seen in Figure 8.20 and Figure 8.32. The overall trend is that the vapor-phase TPH concentration in the region of the soil closest to the inlet decrease first, followed by a decrease in the higher locations at later times. This matches closely with the theory. As the uncontaminated air enters the soil column it becomes saturated with the contaminant present in the soil closest to the inlet. As the contaminant decreases in the lower section of the column the vapor-TPH concentration in the soil gas in the pore space will also decrease. This trend should continue with time until the vapor-TPH levels have decreased in the whole column.

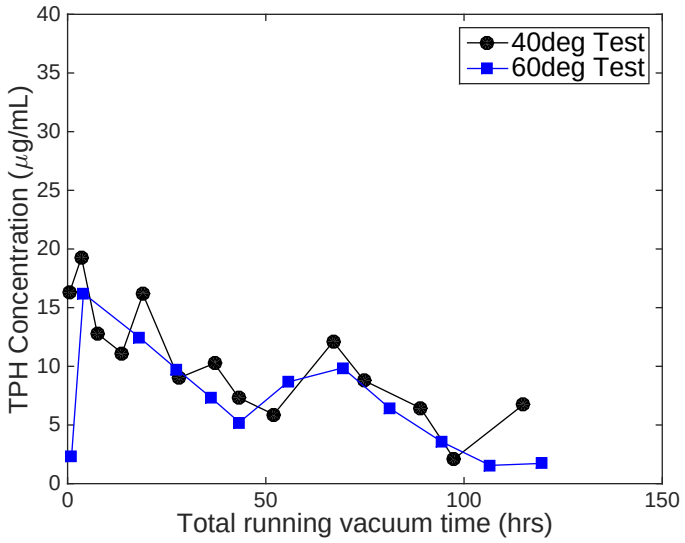

Figure 9.4: A comparison of the TPH concentration of the soil gas in the pore spaces 300 mm above the base of the column

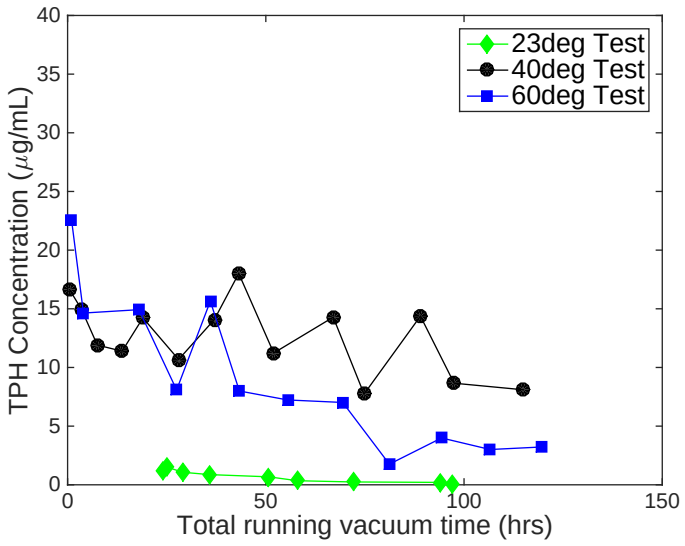

Figure 9.5: A comparison of the TPH concentration of the soil gas in the pore spaces 150-180 mm above the base of the column

Figures 9.6 shows the total mass of TPH removed from the soil after each test. Mass removed is calculated assuming an average flow rate of 500 ml/min for each test. The average flow rate is multiplied by the vapor-phase TPH concentration and then integrated over time. Since the test at 23 °C was run for a shorter period of time, Figure 9.6 shows the total TPH removed for all three tests after approximately 90 hours of applied vacuum. Figure 9.6 also shows the total TPH removed in approximately 120 hours of applied vacuum for the test at 40 and 60 °C tests. The total mass of TPH removed for the 23 °C test (after 90 hrs), 40 °C test (after 120 hrs), and 60 °C test (after 120 hrs) was 0.15, 0.99, and 1.53 g, respectively. This data clearly shows an increase in removal with temperature. It is also interesting to note that the vapor-phase TPH concentration for the 60 °C decreases more rapidly and reaches a lower value than the 40 °C test. This implies that not only is the total TPH removed higher for the test at 60 °C but the rate of removal is also higher. Assuming the TPH concentration in the effluent of the 40 °C test observed after 90 hrs is attributed to the increase in flow rate, and would not have occurred if the flow rate had remained constant, the final vapor-phase TPH concentration of the effluent for all three tests is sufficiently small that further contaminant removal will be very minimal with further vacuum. Thus, by comparing these

values to the original amount of TPH in the soil, the percent of TPH removed from the soil can be calculated. The percentage of the initial TPH in the soil removed for the 23 °C test (after 90 hrs), 40 °C test (after 120 hrs), and 60 °C test (after 120hrs) was 0.04%, 0.24% and 0.37%, respectively. Although this clearly shows an increase of TPH removal with temperature, the overall removal percentage is still very low, even for the 60 °C test. This is likely due to the low volatility of diesel fuel combined with the low permeability of the silt.

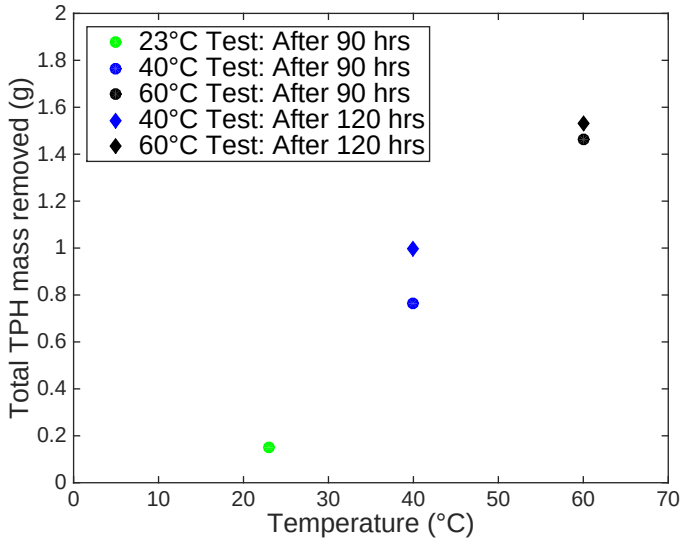

Figure 9.6: Total TPH removed after 90 and 120 hours of applied vacuum

Although there are differences in the boundary conditions between the three tests, the role of temperature is clearly shown in the analysis; the greatest amount of diesel removal occurred in the test with the highest temperature. Unfortunately, the actual percentage of the initial diesel in the soil removed was not significant.

Chapter 10

Conclusion

The goal of this study is to understand the conditions in which heat collected from soil-borehole thermal energy storage (SBTES) systems can be used for thermally enhanced vapor extraction. SBTES systems consist of an array of closely spaced vertical geothermal boreholes, and are used for storing heat collected from solar thermal panels. The temperature of the soil in these systems is expected to reach values ranging from 40 to 60 °C. Although thermal enhancement of soil-vapor extraction (SVE) has been investigated in several studies, they typically involved temperatures in the range of 100 to 300 °C and the role of relatively low temperatures such as those in SBTES systems has not been thoroughly evaluated. Although the temperature is not significant, the heat is from a renewable source and can be applied for a long duration for low cost. The experimental approach used in this study involves column tests in which a vacuum is used to draw air through an unsaturated soil column that has a constant initial distribution in diesel. Three tests were performed in which the soil column was heated to different temperatures. The data collected, including the airflow rates, the soil temperature and dielectric permittivity, and the total petroleum hydrocarbon (TPH) in the gas phase at different locations indicates that moderate increases in temperature lead to small increases in the removal of diesel from the unsaturated soil layer. The major conclusions that can be drawn from this study are:

- The amount of water removed from the column increased with temperature, reflecting an increase in the mass transport for higher temperatures.

- The rate of TPH removed increased with temperature using SVE.
- The amount of TPH removed increased with temperature using SVE.
- Although temperature was observed to lead to a clear increase in the amount of TPH removed from the soil column, the actual percentage of the initial diesel in the soil removed was not significant.

Although this study did show that TPH concentrations in the effluent do increase with moderate temperature increases, the increases observed in the amount removed was not sufficient to lead to a significant change in the percent of initial diesel removed. This is likely due to the low volatility of diesel combined with the low permeability of Bonnie Silt. These results confirm that moderate increases in temperature are not sufficient to significantly improve diesel remediation from a low-permeability silt. Instead, this method should be investigated using more volatile LNAPLs, such as gasoline, where moderate increases in temperature may have a more drastic effect on the TPH concentrations in the effluent, leading to a more significant effect on the rate and amount of TPH removed. The heat collected from SBTES systems is from a renewable source and can be applied for a long duration for low cost. If applied to a soil contaminated with more volatile compounds, it could significantly reduce the remediation time thus decreasing remediation costs considerably.

REFERENCES

Abriola, L., Bradford, S., Lang, J., and Gaither, C. (2004). "Volatilization of binary nonaqueous phase liquid mixtures in unsaturated porous media." *Vadose Zone Journal*, 3(2), 645–655.

Baehr, A. (1987). "Selective transport of hydrocarbons in the unsaturated zone due to aqueous and vapor phase partitioning." *Water Resources Research*, 23(10), 1926–1938.

Banerjee, S. (1984). "Solubility of organic mixtures in water." *Environmental Science & Technology*, 18(8), 587–591.

Baser, T., Lu, N., and McCartney, J. S. (In 2nd review, 2015). "Operational response of a soil-borehole thermal energy storage system." *ASCE Journal of Geotechnical and Geoenvironmental Engineering*.

Baser, T. and McCartney, J. S. (2015). "Development of a full-scale soil-borehole thermal energy storage system." *Proceedings of the International Foundations Conference and Equipment Exposition (IFCEE 2015)*, San Antonio, TX., ASCE, 1608–1617.

Bear, J. (1972). *Dynamics of Fluids in Porous Media*. Elsevier Publishing, New York, N.Y., Chapter: Flow of immiscible Fluids, 439–573.

Brooks, R. H. and Corey, A. T. (1964). "Hydraulic properties of porous media." *Colorado State University, Fort Collins. Hydrology Papers*, (3).

Corey, A. T. (1986). *Mechanics of Immiscible Fluids in Porous Media*. Water Resources Publications, Fort Collins, CO.

Fetter, C. W. (1999). *Contaminant Hydrogeology*. Prentice hall, Upper Saddle River, NJ, Chapter: Multiphase Flow, 207.

Goss, K. (1992). "Effects of temperature and relative humidity on the sorption of organic vapors on quartz sand." *Environmental Science and Technology*, 26(11), 2287–2294.

Heron, G., Zutphen, V. M., Christensen, T. H., and Enfield, C. G. (1998). "Soil heating for enhanced remediation of chlorinated solvents: A laboratory study on resistive heating and vapor extraction in a silty, low-permeable soil contaminated with trichloroethylene." *Environmental Science and Technology*, 32(10), 1474–1481.

Hinchee, R. and Reisinger, H. (1985). "Multi-phase transport of petroleum hydrocarbons in the subsurface environment: theory and practical application." *Proc., Petroleum Hydrocarbons and Organic Chemicals in Ground Water: Prevention, Detection and Restoration*, Dublin, Ohio, National Water Well Association - American Petroleum institute, 58–76.

Hoag, G. and Marley, M. (1986). "Gasoline residual saturation in unsaturated uniform aquifer materials." *Journal of Environmental Engineering*, 122(3), 586–604.

Iezzoni, H. and McCartney, J. S. (In 2nd review, 2015). "Calibration of capacitance sensors for compacted silt in nonisothermal applications." *ASTM Geotechnical Testing Journal*.

Jadhav, R., Amano, R., and Jatkar, J. (2002). "Numerical analysis of heated soil vapor extraction system." *Proc., ASME International Mechanical Engineering Congress and Exposition*, New Orleans, Louisiana, ASME.

Kaluarachchi, J. J. and Mesbah-Ul Islam, K. M. (1995a). "Thermal venting to recover less-volatile hydrocarbons from the unsaturated zone, 1. theory." *Journal of Contaminant Hydrology*, 17, 293–311.

Kaluarachchi, J. J. and Mesbah-Ul Islam, K. M. (1995b). "Thermal venting to recover less-volatile hydrocarbons from the unsaturated zone, 2. model applications." *Journal of Contaminant Hydrology*, 17, 293–311.

Kawala, Z. and Atamanczuk, T. (1998). "Microwave-enhanced thermal decontamination of soil." *Environ. Sci. Technol.*, 32, 2602–2607.

Klinkenberg, L. J. (1941). "The permeability of porous media to liquids and gases." *American Petroleum Institute, Drilling and Productions Practices*, 200–213.

Lingineni, S. and Dhir, V. K. (1992). "Modeling of soil venting processes to remediate unsaturated soils." *Journal of Environmental Engineering*, 118, 135–152.

Lyman, W. J., Reidy, P. J., and Levy, B. (1992). *Mobility and Degradation of Organic Contaminants in Subsurface Environments*. C. K. Smoley, INC., Chelsea, Michigan.

Mackay, D., Shiu, W., and Ma, K. (1992a). *Illustrated handbook of physical-chemical properties of environmental fate for organic chemicals*, Vol. 1. Lewis Publishers, Chelsea, Michigan, Chapter: Monoaromatic Hydrocarbons.

Mackay, D., Shiu, W., and Ma, K. (1992b). *Illustrated handbook of physical-chemical properties of environmental fate for organic chemicals*, Vol. 2. Lewis Publishers, Chelsea, Michigan, Chapter: Polynuclear Aromatic Hydrocarbons (PAHs).

Mackay, D., Shiu, W., and Ma, K. (1993). *Illustrated handbook of physical-chemical properties of environmental fate for organic chemicals*, Vol. 3. Lewis Publishers, Chelsea, Michigan, Chapter: Hydrocarbons.

Marley, M. and Hoag, G. (1984). "Induced soil venting for recovery/restoration of gasoline hydrocarbons in the vadose zone." *Proc., Petroleum Hydrocarbons and Organic Chemicals in Ground Water*, Houston,TX, National Water Well Association-American Petroleum Institute.

McCartney, J., Ge, S., Reed, A., Lu, N., and Smits, K. (2013). "Soil-borehole thermal energy storage systems for district heating." *Proc., European Geothermal Congress*, Pisa, Italy, 10.

Mercer, J. W. and Cohen, R. M. (1990). "A review of immiscible fluids in the

subsurface: properties, models, characterization and remediation." *Journal of Contaminant Hydrology*, 6(2), 107–163.

Newell, N. J., Acree, S. D., Ross, R. R., and Huling, S. G. (1995). "Light nonaqueous phase liquid." *Report No. EPA/540/S-95/500*, Environmental Protection Agency.

Noggle, J. (1985). *Physical Chemistry*. Little Brown, Boston, MA.

Oma, K. H. and Buelt, J. L. (1988). "In situ heating to detoxify organic-contaminated soils." *5th National Conference on Hazardous Wastes and Hazardous Materials*, Las Vegas, Nevada, 154–157.

Park, G., Shin, H., and Ko, S. (2005). "A laboratory and pilot study of thermally enhanced soil vapor extraction method for the removal of semi-volatile organic contaminants." *Journal of Environmental Science and Health, Part A: Toxic/Hazardous Substances and Environmental Engineering*, 40(4), 881–897.

Poppendieck, D. G., Loehr, R. C., and Webster, M. T. (1999a). "Predicting hydrocarbon removal from thermally enhanced soil vapor extraction systems: 1. laboratory studies." *Journal of Hazardous Materials*, B69(1), 81–93.

Poppendieck, D. G., Loehr, R. C., and Webster, M. T. (1999b). "Predicting hydrocarbon removal from thermally enhanced soil vapor extraction systems: 2. field study." *Journal of Hazardous Materials*, B69(1), 95–109.

Rathfelder, K., Lang, J., and Abriola, L. (1995). "Soil vapor extraction and bioventing: Applications, limitations, and future research directions." *Reviews of Geophysics*, 33(S2), 1067–1081.

Rathfelder, K., Yeh, W. W., and Mackay, D. (1991). "Mathematical simulation of soil vapor extraction systems: Model development and numerical examples." *Journal of Contaminant Hydrology*, 8(3-4), 263–297.

Rothenstein, C. (2003). "Statement of cliff rothenstein before the subcommittee on environmental and hazordous materials committee on energy and com-

merce." *Office of Underground Storage Tanks, EPA*.

Tomlinson, D. W., Thornton, S. F., Thomas, A. O., Leharne, S. A., and Wealthall, G. P. (2014). *An Illustrated Handbook of LNAPL Transport and Fate in the Subsurface*. Contaminated Land: Aplications in Real Environments, London, England.

Traore, K. (2013). "Physical modeling of coupled water and heat flow within a borehole heat exchanger array in the vadose zone." M.S. thesis, The University of Colorado at Boulder, USA.

USEPA (1996). *How To Effectively Recover Free Product At Leaking Underground Storage Tank Sites: A Guide For State Regulators*. U.S. Environmental Protection Agency, Chapter: Behavior of Hydrocarbons in the Subsurface.

USEPA (2004). *How To Evaluate Alternative Cleanup Technologies For Underground Storage Tank Sites: A Guide For Corrective Action Plan Reviewers*. U.S. Environmental Protection Agency, Chapter: Soil Vapor Extraction.

Wilhoit, R. and Zwolinski, B. (1971). *Vapor Pressures and Heats of Vaporization of Hydrocarbons and Related Compounds*. Thermodynamics Research Center, College Station, Texas.

Wilkins, M., Abriola, L., and Pennell, K. (1995). "An experimental investigation of rate limited nonaqueous phase liquid volatilization in unsaturated porous media: Steady state mass transfer." *Water Resources Research*, 31(9), 2159–2172.

Wilson, J. L., Conrad, S. H., Mason, W. R., Peplinski, W., and Hagan, E. (1990). "Laboratory investigation of residual liquid organics from spills, leaks, and the disposal of hazardous wastes in groundwater." *Report No. EPA/600/6-90/004*.

Zhendi, W. (2003). "Characteristics of spilled oils, fuels, and petroleum products: Composition and properties of selected oils." *Report No. EPA/600/R-03/072*, Emergencies Science and Technology Division, Environment Canada, Ottawa,

Ontario.

Appendix A

GC Analytical Methods

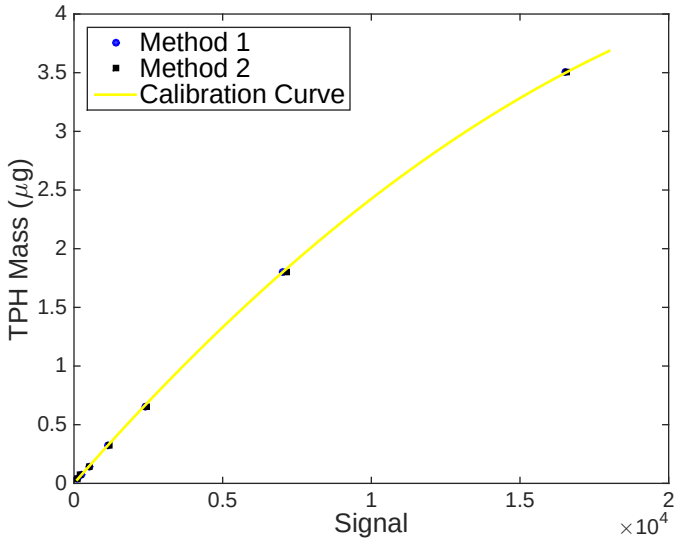

Figure A.1: Calibration chart

Table A.1: Method 1: Used for vapor samples in Test 1

Injection volume	2.5 mL
Front SS Inlet He	
Split/Splitless Mode	Split
Heater	275 °C
Pressure	14.505 psi
Total Flow	8.9596 mL/min
Septum Purge Flow	3 mL/min
Split ratio	10:1 min
Plit flow	5.4178 mL/min
Run Time	35.25 min
Front Detector FID	
Heater	350 °C
H2 Flow	35 mL/min
Air Flow	400 mL/min
Makeup Flow	30 mL/min
Oven Program	
Initial	40 °C hold for 1 min
Ramp 1	then 20 °C/min to 325 °C hold for 20 min
Column 1	
Restek Rxi-1ms:	-837.07816
Restek Rxi-1ms	
330 °C	20 m x 180 μm x 0.18 μm
In	Front SS Inlet He
Out	Front Detector FID

Table A.2: Method 2: Used for vapor samples in Test 2 and Test 3

Injection volume	1 mL
Front SS Inlet He	
Split/Splitless Mode	Split
Heater	275 °C
Pressure	14.505 psi
Total Flow	8.9596 mL/min
Septum Purge Flow	3 mL/min
Split ratio	10:1 min
Spit flow	5.4178 mL/min
Run Time	35.25 min
Front Detector FID	
Heater	350 °C
H2 Flow	35 mL/min
Air Flow	400 mL/min
Makeup Flow	30 mL/min
Oven Program	
Initial	40 °C hold for 1 min
Ramp 1	then 5 °C/min to 100 °C hold for 0 min
Ramp 2	then 15 °C/min to 324 °C hold for 10 min
Column 1	
Restek Rxi-1ms:	-837.07816
Restek Rxi-1ms	
330 °C	20 m x 180 μm x 0.18 μm
In	Front SS Inlet He
Out	Front Detector FID